DOT PHMSA

Final Public Report No. 16-015

Public report on:

# Improve and Develop ILI Tools to Locate, Size, and Quantify Complex/Interacting Metal Loss Features and Dents

Bruce Nestleroth, Kiefner, and
James Simek, TD Williamson

April 26, 2016

0339-1301

Intentionally blank

Final Public Report No. 16-015

**Final Public Report**

on

# IMPROVE AND DEVELOP ILI TOOLS TO LOCATE, SIZE, AND QUANTIFY COMPLEX / INTERACTING METAL LOSS FEATURES AND DENTS

to

## US DEPARTMENT OF TRANSPORTATION
## PIPELINE AND HAZARDOUS MATERIALS SAFETY ADMINISTRATION

**Contract Number:**
**DTPH56-13-T-000009**

**April 26, 2016**

**Prepared by**


**Bruce Nestleroth, PhD**
**Technical Authority**


**Approved by**


**Dyke Hicks**
**Senior Principal Engineer**

**Kiefner and Associates, Inc.**
**4480 Bridgeway Avenue, Suite D**
**Columbus, OH 43219**


0339-1301

## DISCLAIMER

This document presents findings and/or recommendations based on engineering services performed by employees of Kiefner and Associates, Inc. The work addressed herein has been performed according to the authors' knowledge, information, and belief in accordance with commonly accepted procedures consistent with applicable standards of practice, and is not a guaranty or warranty, either expressed or implied.

The analysis and conclusions provided in this report are for the sole use and benefit of the Client. No information or representations contained herein are for the use or benefit of any party other than the party contracting with Kiefner. The scope of use of the information presented herein is limited to the facts as presented and examined, as outlined within the body of this document. No additional representations are made as to matters not specifically addressed within this report. Any additional facts or circumstances in existence but not described or considered within this report may change the analysis, outcomes and representations made in this report.

## ACKNOWLEDGEMENTS

Kiefner and TD Williamson would like to thank our pipeline company partners Koch Pipeline Company, Shell Pipeline Company, Phillips 66 and Conoco Phillips for supplying ILI data and permitting access to excavation sites to attain the data used in these developments. Data from actual pipeline anomalies was crucial in this process.

## TABLE OF CONTENTS

INTRODUCTION ..... 1
SUMMARY AND CONCLUSIONS ..... 2
BACKGROUND ..... 3
Corrosion assessment by MFL ..... 3
General Advancement in ILI technology ..... 4
Dent Assessment by ILI ..... 4
Seam Corrosion Assessment by ILI ..... 6
APPROACH ..... 7
PIPE SAMPLES ..... 8
Dent Discrimination ..... 9
Selective seam weld corrosion ..... 10
Metal loss ..... 10
ALGORITHM DEVELOPMENT ..... 10
Algorithm for Dent Discrimination ..... 10
Algorithm for SSWC Discrimination ..... 18
Algorithm for Classifying Complex Corrosion ..... 24
Algorithm for Sizing Complex Corrosion ..... 38
VERIFICATION ..... 47
REFERENCES ..... 54
ATTACHMENT A - FULL LISTING OF CLASSIFIER INPUTS AND PREDICTIONS USING OUT-OF-BAG SAMPLE ..... 56
ATTACHMENT B - DETAILED DATA AND RESULTS FOR SSWC MODEL DEVELOPMENT ..... 60

## LIST OF TABLES

Table 1. Classifier input feature importance ..... 14
Table 2. Classifier confusion matrix ..... 16
Table 3. Classifier performance summary ..... 16
Table 4. EDM Notch Burst Tests ..... 51

## LIST OF FIGURES

Figure 1. Pair plot of some of the classifier inputs for the three metal loss types ..... 13
Figure 2. Precision and recall for the three metal loss types as a function of gouge probability threshold ..... 16

Figure 3. Metal loss sizing performance for anomalies in dents.....18

Figure 4. Pair plot of the nondimensionalized classifier inputs for the two classes. Red squares represent SSWC, and blue circles represent CCLS. .....20

Figure 5 Receiver operating characteristic for the SSWC classifier.....22

Figure 6. SSWC depth model performance .....23

Figure 7. SSWC length model performance.....24

Figure 8. A complex corrosion patch as detected by (a) MFL sensors (b) SMFL sensors and (c) laser scanning of the pipe surface .....26

Figure 9. (a) Part of the MFL data of a whole joint that was later scanned by laser. (b) Interactively marked regions of interest showing complex corrosion patch.....27

Figure 10. Four complex corrosion patches in an MFL joint with the peaks of individual pits marked. Colored dots placed on deepest points of the local pits were automatically identified. .....28

Figure 11. Peaks identified in the complex corrosion patches of MFL data are mapped onto SMFL data with corresponding scaling, translation and local window search.....30

Figure 12. The MFL pits segmentation by a constrained region growing method in the four complex corrosion patches of the MFL data.....32

Figure 13. Result of individual pit segmentation in SMFL data. Each pit has a direct correspondence with pits in MFL. Pits in SMFL have a corresponding pit in MFL with a same label. .....33

Figure 14. The peaks of MFL are mapped to low resolution laser data of complex corrosion patches.....35

Figure 15. Peaks marked on full resolution laser data of the complex corrosion patches.....36

Figure 16. The pits segmented in laser data using the pits identified in MFL data. Many pits in the laser data have gone unmarked (white areas) as those pits are either not identified in MFL data or merged with other pits in the lower resolution MFL data. .....37

Figure 17. A complex corrosion patch as detected by (a) MFL sensors (b) SMFL sensors and (c) laser scanning of the pipe surface .....40

Figure 18. Labeling and matching ILI pit regions to laser data pit regions .....41

Figure 19. A complex corrosion patch in the laser data segmented and labeled to match corresponding pits in the MFL data.....42

Figure 20. Approximate distribution of ground truth measurements from laser data.....43

Figure 21. Unregularized model performance .....46

Figure 22. Regularized model performance.....47

Figure 23. Dent with gouge, identified by classification algorithm, that was subjected to repeated pressurization to SMYS.....49

Figure 24. The dent depth in percent.....50

Figure 25. Metallographic section through flaws G1 (left) and G5 (right).....52

Figure 26. Metallographic section through flaw G8 groove .....52
Figure 27. Typical blunt machined groove .....53

Intentionally blank

# Improve and Develop ILI Tools to Locate, Size, and Quantify Complex/Interacting Metal Loss Features and Dents

Bruce Nestleroth, Kiefner and James Simek, TD Williamson

## INTRODUCTION

The ability to characterize metal loss and gouging associated with a dent, the identification of corrosion type near the longitudinal seam, and interacting and complex corrosion geometries are three of the remaining obstacles with in-line inspection (ILI) integrity assessment of metal loss defects. The difficulty with denting is that secondary features of corrosion and gouging present very different safety and serviceability scenarios; corrosion in a dent is often not very severe while metal loss caused by gouging can be quite severe. Selective seam weld corrosion (SSWC) of older low frequency electric resistance welding (ERW) seams also presents two different integrity scenarios; the ILI tool must differentiate the more serious SSWC condition from the less severe conventional corrosion which just happens to be near a low frequency ERW seam. Both of these cases involve identification difficulties that require improved classification of the anomalies by ILI to enhance pipeline safety.

In the last decade, the detection capability for ILI tools has improved, enabling the reporting of smaller corrosion and shallower dents. Also, many tools are better at detecting the seam weld in well-trimmed ERW pipe. However, the reporting of smaller corrosion that is coincident with dents or the long seam has caused an increase in excavations per the regulations. The goal of the regulations is to ensure that mechanical damage in dents and selective corrosion of the long seam, both potentially service limiting anomalies, are always detected.

Keeping with the spirit of the regulations, the goal of the work presented herein is to build classifiers that combine the measurements from multiple sensing systems. These classifiers, when implemented in data analysis software tools, will be used to detect mechanical damage in dents and selective corrosion of the long seam, while dismissing many of the smaller corrosion features that do not impact pipeline performance. The classifiers are designed to be conservative, meaning some non-injurious corrosion anomalies will be designated for excavation so that the likelihood of catching all potentially injurious mechanical damage and selective seam corrosion is greater. This report discusses the development and verification of these classifiers.

The third topic this work is improvements to corrosion depth determination by magnetic flux leakage (MFL). MFL tools size most metal loss anomalies with sufficient accuracy to achieve acceptable pipe integrity. However some corrosion geometries provide a greater challenge to achieve the specified accuracy. One anomaly class is wide spread corrosion with pitting corrosion in large patches of general corrosion. This report also discusses the development of improved sizing models.

## SUMMARY AND CONCLUSIONS

Three new classifiers are presented for MFL tools, the technology most commonly used by pipeline operators for integrity assessments. The dent classifier that distinguishes dents with gouges from dents with corrosion or smooth dents uses a high and low magnetization level approach combined with a new method for analyzing the signals. In this classifier, detection of any gouge signal is paramount; the conservatism of the classifier ensures reliable identification of gouges can be achieved. In addition to the high and low field data, the classifier uses the number of distinct metal loss signatures at the dent, the estimated maximum metal loss depth, and the location of metal loss signatures relative to dent profile (e.g. Apex, Shoulder).

The SSWC classifier that distinguishes SSWC from corrosion near the longitudinal weld uses two orientations of the magnetic field, the traditional axial field and a helical magnetic field. In this classifier, detection of any long narrow metal loss is paramount; the conservatism of the classifier ensures high identification of SSWC can be achieved. The relative amplitude of the corrosion signal for the two magnetization directions is an important characteristic, along with length and width measures of the corrosion features.

The third classifier for complex and interacting metal loss is a longer development. The SSWC and dent with metal loss classifiers mainly examined detection of these anomalies. Detection algorithms primarily require data from smaller anomalies to demonstrate the effectiveness for detection. Metal loss sizing algorithm development requires data from all sizes of corrosion, from small inconsequential to large repairable anomalies. The available data was sufficient to develop a frame work for a new sizing model for metal loss. Additional inspection and excavation confirmation data are required to complete the algorithms.

These models were developed using ILI data from pipeline anomalies identified during actual inspections, a critical step to ensure results can be directly transferred into practice. Inspection measurements from excavations as well as pipe removed from service for lab analysis and pressure testing were used to confirm the results.

# BACKGROUND

The most common pipeline inspection method, magnetic flux leakage (MFL), uses magnetic components to induce magnetic flux within the pipeline wall [1]. The magnetic flux naturally enters the metal wall of the pipeline and distributes evenly to produce a full volumetric inspection. Anomalies in the wall of the pipeline tend to disrupt the uniform flow of the flux and create a leakage of magnetic flux, which can then be detected by sensors. MFL-based tools have the capability of addressing many of the threats listed in ASME B31.8S. Each implementation of MFL technology typically focuses on a subset of pipeline wall anomalies that affect pipeline integrity with varying levels of success, or sensitivity, for each implementation. Not all implementations will provide sufficient information for detailed defect assessment.

## Corrosion assessment by MFL

MFL-based inspection tools for detecting corrosion commonly use high magnetic fields to saturate the pipeline material. Such high magnetic field-based magnetizers help suppress noise due to local stress variations and changes in the microstructure of the metal [2]. At metal-loss defects, such as corrosion, an increased amount of magnetic flux attempts to flow through the remaining material; however, some flux leaks from the pipeline wall due to saturation of the remaining material. In addition, a second phenomenon causes even more flux to leak. In magnetically saturated materials, an increase in magnetizing flux causes the flux-carrying capability (permeability) to decrease [3]. The combination of increased flux and decreased flux-carrying capacity, which are nonlinearly related, result in significant flux leakage at corrosion anomalies. Furthermore, since flux prefers to stay in the pipe, the flux goes around the anomaly rather than leak out of the pipe.

One of the most challenging anomalies for traditional MFL are long, narrow, axially aligned anomalies sometimes called grooving corrosion. In the mid-1990s, a new type of MFL tool was developed that aligned the magnetic field in the circumferential direction [1]. While this technology improved sizing of grooving corrosion, the sizing of other anomalies types such as patch corrosion and pitting corrosion was better left to traditional axial MFL. Some ILI vendors that supply both tool types combine the two data sets, but this requires the operational logistics and cost of two tool runs.

With all of the limitations of MFL, the rugged nature of the technology make it the most used inspection technology; detection of corrosion is good, however determining the depth corrosion anomalies can be challenging. The specification vendors used for sizing was established in the 1990s and described in the API 1163 ILI standard. In general, the depth of corrosion anomalies is measured to an accuracy of ±10 percent of the wall thickness. For most tool runs, this ±10 percent sizing goal is attained for 80 percent (4 of 5) of corrosion anomalies, in

statistical terms referred to as the certainty. Also in statistical terms, “most tool runs” is defined as the confidence; vendors generally specify a the confidence that a tool run will make specification is about 95 percent , but 5.0 percent (1 of 20) will not make specification. The goal of this work is to improve on these statistical measures; this could be improving the sizing accuracy, decreasing the uncertainty in the measurement accuracy and/or increasing the confidence that the tool will make specification.

## General Advancement in ILI technology

The 1990s was a period when ILI technology was evolving from low resolution, dozens of sensors, to high resolution, hundreds of sensors. This was true for both magnetic flux leakage for detection and sizing of metal loss and caliper tools for the detection and sizing of dents. Advances in computer and data storage technology have enabled many of the improvements. For example, in 1995, a 500 Megabyte (0.5 Gigabytes) of flash memory cost $10,000 and came in a 4 x 4 x 0.5-inch cube; a 16 Gigabyte USB thumb drive is now available for less than 10 dollars. Therefore data storage is less of a limiting factor in ILI tool design.

The technology used in the most common implementation of MFL and caliper tools has matured and is available from many ILI vendors. Most vendors only supply tools that meet the high resolution category. With this higher resolution comes the ability to detect much smaller anomalies:

- Dents with depth greater than 0.5% of pipe diameter can be detected where low resolution tools detected dents greater than 2%.
- Metal loss on the order of 5% of wall thickness can be detected where low resolution tools detected corrosion greater than 20%.

With this higher resolution, ILI tools are identifying many more dents and dents with metal loss. While the MFL tools can detect metal loss associated with gouging, MFL cannot easily and routinely distinguish between metal loss by corrosion and metal loss from gouging. Therefore, many more metal loss anomalies in dents must be investigated after an ILI run today than when the regulation was first implemented in 2000.

## Dent Assessment by ILI

Accepted codes, standards, and governmental regulations address the secondary features of corrosion and gouging in dents. As an example, per 49 CFR 192.933 (d) natural gas pipeline operators in the United States “…must treat the following conditions as immediate repair conditions: (ii) A dent that has any indication of metal loss, cracking or a stress riser.” A similar requirement can be found for liquid pipelines in 49 CFR 195.452(h)(4) “(i) immediate repair conditions (C) dents on the top of the pipeline (. . .) with any indicated metal loss.”

The regulations were shaped by three incidents in the 1990s in which the pipeline failure mode was attributed to dents with gouging. These failures highlighted the need to detect gouging associated with mechanical damage. Gouges, as defined by API 1160, are “the elongated grooves or cavities usually caused by mechanical removal or smearing of metal”. While the detection of metal loss in a dent is possible, detection of the metal loss associated with a gouge may not always be detected by conventional MFL tools, especially if the gouge is long and narrow. In two of the three incidents, the pipelines had been inspected by MFL pigs, and post failure analysis of the data showed a metal loss anomaly present in the dent.

Dents, which are primarily detected by caliper tools, can be caused by excavation equipment. Therefore, dents with associated metal loss could have gouging. But, more often than not, the metal loss in a dent is caused by corrosion at damaged or disbonded coating. Unfortunately, traditional applications of MFL tools cannot reliably discern gouging from simple metal loss due to corrosion.

## Dual Field Magnetization Theory

An alternative MFL approach that was developed with DOT PHMSA funding, dual field MFL, can distinguish dents with gouges from dents metal loss [7]. This technology has been commercialized in different forms by ILI vendors. The high magnetic field-based magnetizers commonly used [1] suppress noise due to local stress variations and changes in the microstructure of the metal [2]. These stress and material variations are indicative of mechanical damage and since they change the flux-carrying capacity of the pipe [4-5], they can be detected with a properly designed tool. A local decrease in flux-carrying capacity causes leakage similar to that resulting from metal-loss defects. A local increase in flux-carrying capacity causes a decrease in flux leakage relative to the nominal, magnetic field level. For example, for tensile stresses, the overall flux levels in the pipeline increase. However, for compressive stresses, such as cold-worked areas, the flux levels decrease. The flux density variations between tensile stresses and compressive stresses are small for magnetic field levels greater than approximately 6,400 A/m (80 Oersted) and nearly negligible for magnetic field levels greater than approximately 9,600 A/m (120 Oersted) depending the magnetic properties of the pipe.. These general values may vary with pipeline wall thickness, chemical composition, grain structure, and fabrication methods [6]. As discussed previously, most MFL-based apparatuses for corrosion are designed to operate above these levels to reduce signals due to stress, typically considered noise. To detect changes in stress and cold working in the pipe wall, however, the magnetic field must be at lower, unsaturated levels, typically between 4000 and 5600 A/m (50 and 70 Oersted). Unfortunately, field levels in this range can produce results that are difficult to interpret because they can be affected by corrosion anomalies, stresses, and changes in material composition. A low-field-strength MFL based pig can be used to detect stresses and material variations using fields in the range of 4000 and 5500 A/m (50 and 70

Oersted); however, corrosion anomalies are also detected at this field level and assessment of these anomalies would be inaccurate as demonstrated by early MFL pigs.

Thus, using two magnetic field levels and methods to process both signals can improve the detection and assessment of pipeline anomalies [7-11]. The high magnetic field employed in most inspection tools detects and sizes metal loss such as corrosion. A second low magnetic field must also be applied to detect the metallurgical changes caused by mechanical damage (e.g., from excavation equipment). To apply a two magnetization approach, it is possible (but rarely practical) to send more than one pig separately through the pipeline. A single pig having two separate sets of magnetizers, while also technically feasible, results in a longer ILI tool that can be prohibitive for some pipeline systems.

## Seam Corrosion Assessment by ILI

Similar to dents, accepted codes, standards and governmental regulations address corrosion near the longitudinal seam weld. For example, per 49 CFR 195.452(h)(4)(iii)(H) liquid pipelines operators in the United States must address corrosion of or along a longitudinal seam weld in 180-days. The primary concern of these regulations is selective seam weld corrosion (SSWC), which accounts for about 1.0 percent of the failure incidents reported in the United States [12]. SSWC is a localized corrosion attack along the bond line of some low-frequency ERW and electric flash welding (EFW) piping that leads to the development of a narrow groove. Since the weld bond line chemistry may be more susceptible to corrosion processes, the presence of corrosion at the weld is considered an indicator of potential SSWC. This is particularly true if the pipeline has the following conditions present:

- Exposure to corrosive conditions due to poor or absent coating;
- Ineffective cathodic protection; and
- The presence of non-metallic inclusions in the weld bond line region (e.g., contaminants present during the manufacturing process).

SSWC is generally not considered to be a concern for pipe manufactured subsequent to 1970 due to the use of cleaner steels with greatly reduced sulfur contents and the replacement of low frequency welding equipment with high frequency equipment in the manufacturing process.

Pipeline companies use in-line inspection (ILI) technology to detect and assess the potential impact of various corrosion threats. SSWC is detectable with both liquid coupled angle beam ultrasonic crack detection (UTCD) and electromagnetic acoustic transducer (EMAT) ultrasonic methods when anomalies are isolated. However, when surface corrosion surrounds the SSWC, detection and sizing can be impacted. For UTCD methods, the adjacent corrosion may change the reflection angle, so energy that reflects from an anomaly may not return to the sending sensor for detection, identification and sizing. EMAT methods detect both the general corrosion

and selective corrosion; however, the long wave length nature of these tools make it difficult to always distinguish between the two corrosion types.

Circumferential MFL methods are most applicable for SSWC since this feature has width. Tight cracks such as stress corrosion cracking or fatigue cracks are difficult to detect with MFL methods. The signal amplitude is a function of crack width combined with length and depth, so sizing of SSWC is not as accurate as other corrosion anomalies. One circumferential tool vendor specifies an accuracy of ±20 percent for axial slotting between 0.2 inch and 0.4 inch in width. Most SSWC anomalies are narrower than this width and nearby corrosion impacts detection, identification and sizing.

In summary, the regulatory requirement of investigating any corrosion of or along a longitudinal seam weld is the result of the difficulty that ILI tools have with detecting and identifying SSWC. The industry and public would benefit if ILI tools could reliably differentiate the more serious SSWC condition from the less severe conventional corrosion near a low frequency ERW seam. These ILI tool limitations require improved anomaly classification algorithms to better identify dents with gouges and SSWC.

## APPROACH

Five different ILI measurements made on a single tool were used to develop the discrimination algorithms:

- Conventional axial MFL technology (high field)
- ID versus OD discrimination sensors
- Deformation measurements
- Helical MFL technology
- Reduced field axial MFL measurements (low field)

The advantage of using data from a single tool run is to avoid the additional step of aligning the data between runs. The goal of this work was to develop algorithms that combine all five methods to differentiate severe mechanical damage from less severe metal loss in dents, separate SSWC from general corrosion near the long seam, and provide better depth characterization of corrosion anomalies.

Previous algorithms for dents with metal loss and gouging attempted to quantify mechanical damage severity. The algorithms established five levels of importance from benign to severe; however this approach was not implemented by industry nor accepted by regulators; one reason was the severity level could not be confirmed without significantly more testing of pipe pulled from service. The more conservative approach presented herein considers all mechanical

damage anomalies to be severe. As the process evolves and improved mechanical damage assessment methods become robust, the assessment of mechanical damage from ILI data may become part of the process. For the SSWC challenge, combining helical and axial MFL should allow metal loss on an ERW longitudinal seam to be identified and better characterized by determining the exact location with respect to the seam and improving sizing algorithms for corrosion associated with the seam. To improve corrosion sizing, corrosion areas identified by ILI were excavated and detailed depth data for the entire area was recorded using an optical method. Algorithms were developed by comparing the optical data sets to the MFL and SMFL Raw signals.

Use of data from actual pipeline anomalies collected at excavation sites was a key part in this development. The results from ILI tool runs and in-the-ditch field assessment data were correlated with ILI data. Pipes were removed from service and burst tests were conducted to determine the remaining strength for selected anomalies. For the dent discrimination classifier, field samples were augmented with some carefully manufactured mechanical damage features.

## PIPE SAMPLES

The key to developing improved algorithms is the collection of in-ditch field data to correlate with ILI data. Pipelines with specific ILI anomalies were targeted for in-ditch measurements, specifically selective seam corrosion, corrosion near the long seam, wide area corrosion, and dents with corrosion or mechanical damage. The pipeline company participants in this project performed excavations on these pipelines. ApplusRTD technicians performed detailed excavations. Dent depth measurements, curvature to determine strain, and etching to detect changes in metallurgy and hardness measurements in dents to detect cold working were used to characterize dents with metal loss and potential gouging. Selective seam weld corrosion anomalies were assessed with replication methods, seam susceptibility measures, field metallurgical assessments and advanced ultrasonic methods to assess depth. Laser Scan data from external corrosion areas were collected for comparison to metal loss data from the multiple measurement ILI tool. Pipeline examined at excavation sites were:

Pipeline A: On a 24-inch pipeline with dents with corrosion, mechanical damage and weld repairs, more than 40 anomalies were targeted.

Pipeline B: On a 6-inch pipeline with corrosion near the seam weld with potential selective seam weld corrosion, 9 anomalies were targeted for the potential of selective seam weld corrosion.

Pipeline C: On a 12-inch pipeline with corrosion near the seam weld with potential selective seam weld corrosion, 7 anomalies were targeted for the potential of selective seam weld corrosion.

Pipeline D: On a 16 inch pipeline with complex corrosion, 13 metal loss features at two locations were targeted.

Pipeline E: On the 3 segments of a 20-inch pipeline with complex corrosion and dents with potential mechanical damage, 4 sites with complex corrosion and 5 dents with metal loss were targeted.

The two pipes for pull testing were:

Pipe F: Mechanical damage pipe sample. A 16-inch pipe was pulled from service and intentionally struck with a backhoe 30 times.

Pipe G: Pitting corrosion pipe sample. This 12-inch pipe, pulled from service, had many significant internal corrosion pits.

## Dent Discrimination

Data were collected from more than 30 excavations on pipelines with dents with corrosion, mechanical damage and weld repairs. These excavations continued through February of 2014. In-the-ditch measurements included dent depth, curvature, strain, gouge assessment, cold work detection by etching, hardness testing, and corrosion depth. Detailed data was collected from more than 40 excavation sites where the ILI analysis identified dents with metal loss, some with potential gouging. In-the-ditch measurements included dent depth, curvature, strain, gouge assessment, cold work detection by etching, hardness testing, and corrosion depth.

Excavations of a 20 inch with pipeline with complex corrosion and dents with potential mechanical damage were performed as this part of the pipeline was undergoing other scheduled maintenance. Three dig sites were dents, with one site having significant mechanical damage. A forth dig site has corrosion.

The dent with metal loss and gouging data bases was augmented with pipe removed from service and intentionally dented with a backhoe. The dents with gouges assessed in the ditch had only small amounts of gouging. This pipe added 30 more dents showing significant gouging.

### Selective seam weld corrosion

Detailed data was collected from more than nine excavation sites where the ILI analysis identified potential selective seam weld corrosion (SSWC). This involved two pipelines, a 6-inch diameter line inspected in 2013 and a 12-inch diameter line inspected in 2012. In the ditch measurements included corrosion depth, grooving ratio, chemical composition and seam susceptibility were assessed. Only the 6-inch line contained SSWC.

### Metal loss

Excavations on a 16-inch pipeline with complex corrosion were performed in March 2014 as this part of the pipeline was undergoing other scheduled maintenance. For the two dig sites, one site was approximately 80 feet, with multiple complex corrosion anomalies. Also at the long site were two preferential seam weld corrosion anomalies.

Another set of metal loss data came from a pipe with significant internal corrosion pulled from service, Pipe G. The 12-inch MDS tool was pulled through this internal corrosion pipe sample five times yielding sufficient data to develop methods for assessing repeatability and variability of depth sizing results. Paired comparisons among the depth measurements for the five pulls show reasonable repeatability pull-to-pull and reasonable variation with respect to the AUT measurements for 139 anomalies. The data were also used to improve MDS Depth performance further by extracting additional information from the combined MFL and SMFL signatures.

## ALGORITHM DEVELOPMENT

### Algorithm for Dent Discrimination

Previous work on dents with gouges and the use of two MFL field levels for prioritization demonstrated a process for identifying signal characteristics that were indicative of cold work and metal removal during the gouge creation [13]. The gouges used in that study were severe, both in depth and length, and obvious “gouge” and “plow” signatures were discernable in the low-field MFL (LFM) signatures after a suitable signal decoupling algorithm was applied. To meet the goal of detecting all mechanical damage, the gouges in the current study were generally shallow and much less severe. Most ILI tools in use today are quite capable of detecting very shallow metal loss. That said, the resulting MFL and LFM signatures were very small and subtle. Signal decoupling was attempted early on in this study but was deemed unreliable because of the strong sensitivity to alignment between the two MFL and LFM data sets. Shifts in sample alignment in both axial and circumferential directions were often as significant as the decoupled signal. Consequently a new approach was required.

Metal Loss Types. The field measurements describe dents with five distinct metal loss types (and associated number of occurrences):

- Corrosion (24)
- Gouge (50)
- Mill Grinding (1)
- Puddle Weld (3)
- No Metal Loss (14)

It was determined that the puddle weld ILI signatures would be sufficiently recognizable as something other than true metal loss in future inspections, and these samples were eliminated from the list, removing one type entirely. A single mill grind sample is insufficient to adequately train a classifier, so this sample was also removed from consideration, leaving 88 of the original 92 samples, and three of the original five types. The remaining three types in the discussion are labeled as follows below:

- Corrosion
- Gouge
- None

**Feature Engineering**. The selection of type labels addressed the problem of choosing meaningful input features. LFM can identify locations where magnetic permeability has changed as a result of cold work. At a gouge enough through-the-thickness cold work will have to take place in order for a LFM signature to be affected significantly. The LFM also has a response associated with bulk metal loss, so a method for separating the LFM response due to permeability versus the LFM response due to removed metal when both LFM and MFL responses are already quite small was needed.

As discussed earlier, full signal decoupling was deemed unreliable for this study because of the small signal sizes. However, it was decided that the ratio of MFL response to LFM response amplitudes might be a suitable stand-in as an indicator of how much the observed LFM signal is due to bulk metal loss versus magnetic permeability change. First, the signal amplitude in the LFM and MFL signals are normalized by their local background level to account for local magnetization strength.

$$\begin{aligned} \mathbb{A}_{lfm} &= \frac{A_{lfm}}{B_{smfl}} \\ \mathbb{A}_{mfl} &= \frac{A_{mfl}}{B_{mfl}} \end{aligned} \tag{1}$$

Then an overall amplitude ratio is computed using these normalized amplitudes as:

$$\mathbb{A}_{ratio} = \frac{\mathbb{A}_{mfl}}{\mathbb{A}_{lfm}} \quad (2)$$

This amplitude ratio is used as an input to the classifier. In practice, whenever $\mathbb{A}_{lfm}$ is zero, $\mathbb{A}_{mfl}$ is also zero. Under these circumstances, $\mathbb{A}_{ratio}$ is set to zero by definition. Other feature inputs from the ILI record are:

- Number of distinct metal loss signatures at the dent (ML Sig Count)
- Estimated maximum metal loss depth (ML Depth %)
- Location of metal loss signatures relative to dent profile (Apex, Shoulder, Both, or None)
- The location data are first converted to binary indicator variables before classifier training.

Just as important in this study are the features which were eliminated from consideration. Orientation with respect to top-of-pipe was not included in the feature set since the manufactured dents do not have a meaningful orientation, and those dents constitute a significant fraction of the samples in this study. Dent depth was also excluded since dent depth was strongly correlated with real versus manufactured anomalies. The dents from operating pipelines were all very shallow. The dents in the manufactured set were generally deeper. Dent depth was removed to avoid the potential of the classifier exploiting this somewhat artificial correlation that happens to be present in this data set but would not be representative of the general mechanical damage population in actual use.

The classifier input features are plotted as pairs against each other in Figure 1. The separation between the classes is quite subtle, and simple linear decision boundaries would be insufficient to provide good classifier performance. A more advanced classification model is appropriate.

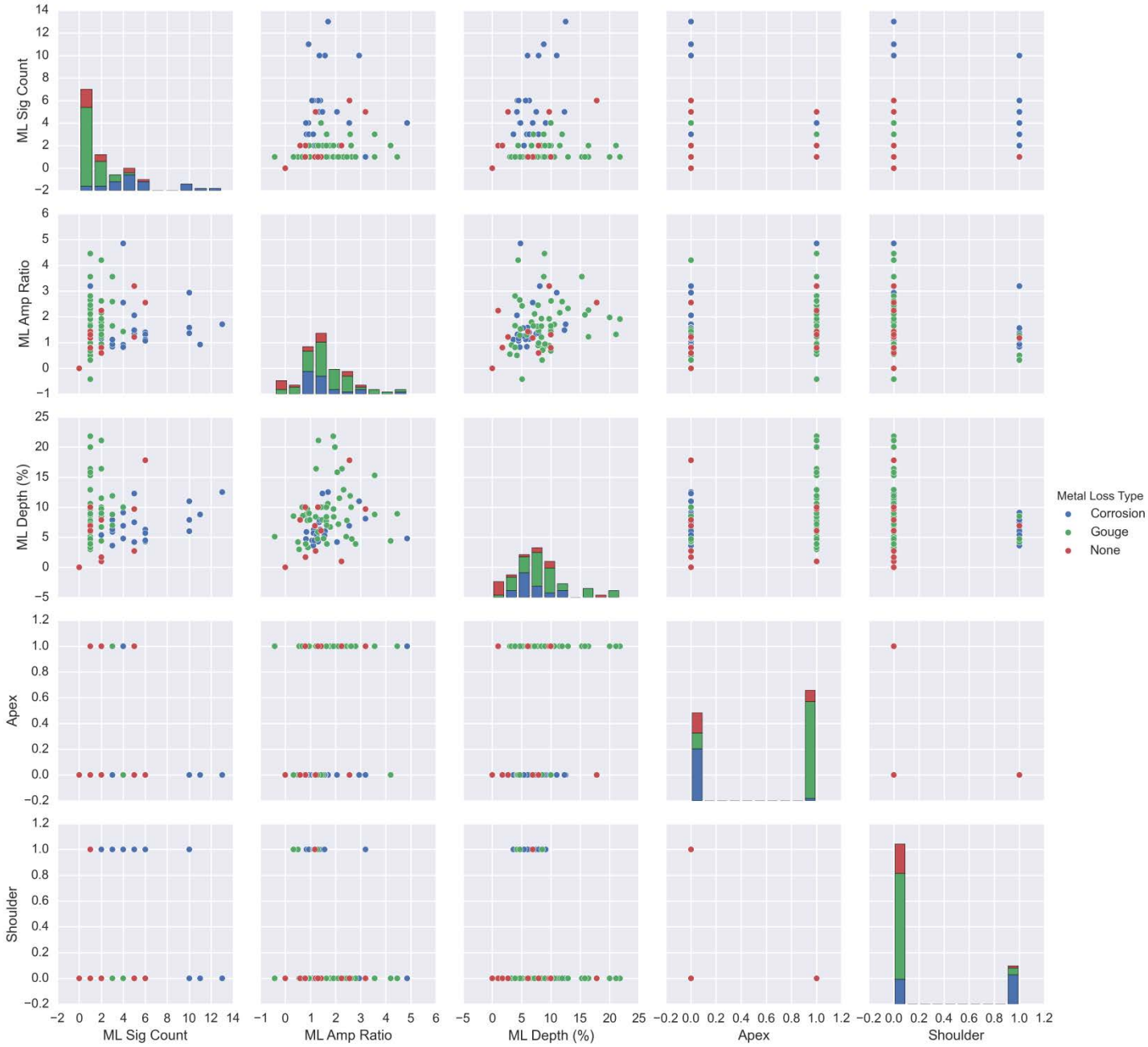


**Figure 1. Pair plot of some of the classifier inputs for the three metal loss types**

**Model Selection**. A random forest classifier was selected because of its ability to model a complex decision boundary while still avoiding the tendency to over fit the training data. Random forests are created by training many binary decision trees in a special fashion and then averaging the predictions of these trees. A full discussion can be found in the literature and is beyond the scope of this paper [14]. When trained with a technique called "bootstrap aggregation," random forest classifiers generate their own estimates of generalization accuracy based on samples that are excluded from the training of individual trees in the ensemble. These samples are sometimes referred to as "out-of-bag" (OOB) samples. We take advantage of this feature in the performance metrics that follow.

**Model Training.** A random forest classifier with 100 individual binary tree estimators was trained on the 88 observations with the goal of predicting the three metal loss types: Corrosion, Gouge, and None. Increasing the number of trees beyond 100 produced no obvious improvement in classifier performance.

The classifier itself estimates the relative importance of the various input features as part of the training process. Table 1 shows relative input feature importance for the metal loss classifier. Metal loss signal count, amplitude ratio, and estimated metal loss depth appear to be of nearly equal importance while metal loss location indicator variables are somewhat less important unless the metal loss is located at the apex of the dent.

**Table 1. Classifier input feature importance**

| Input Feature | Relative Importance |
|---|---|
| **ML Sig Count** | 0.25 |
| **ML Amp Ratio** | 0.22 |
| **ML Depth (%)** | 0.21 |
| **Apex** | 0.17 |
| **Both** | 0.05 |
| **None** | 0.02 |
| **Shoulder** | 0.08 |

**Custom Decision Function**. In a multi-class problem such as this one, the classifier produces a probability that each observation belongs to each of the types. With type probabilities in hand, the most commonly used decision function is to assign each observation to the type that has the highest probability. However, in this study we wish to influence the decision function to err on the side of assigning observations to the "Gouge" type to be conservative. As a result, we adopt a decision function that assigns each observation to whichever type has the highest probability except where the probability of "Gouge" is above a certain threshold in which case "Gouge" is assigned.

As a brief illustrative example, consider that the classifier might return the following type probabilities after evaluating the feature inputs for a given sample:

- Corrosion: 0.45
- Gouge: 0.35
- None: 0.20

The conventional decision function would assign this sample to the “Corrosion” type since its probability was the highest. However, to reflect a desire for conservatism, suppose the decision function is modified to assign “Gouge” to any sample that has a gouge probability above 0.3 regardless of the other type probabilities. For this sample the more conservative decision function would assign this sample to the “Gouge” type.

More precisely, there are quantitative measures of classifier performance that are useful to examine in this study (see [14]).

> *Precision*: The fraction of samples that were correctly called “type” out of all samples that were called “type.”
>
> *Recall*: The fraction of samples that were correctly called “type” out of all samples that were truly “type.”

Under these definitions, high precision implies a low false positive rate, and high recall implies a low false negative rate. The simultaneous maximization of both is generally not possible. We would seek to maximize precision when calling false positives would be most detrimental. Conversely, we seek to maximize recall when false negatives would be most detrimental. A classifier with high precision might be labeled as efficient while a classifier with high recall might be labeled as conservative.

**Out-of-Bag Performance Metrics**. As discussed previously, the OOB samples in a random forest model can be used to provide unbiased estimates of classifier performance similar to what would be obtained through the use of a hold-out test set. The OOB samples are used first in the selection of a suitable gouge probability threshold followed by a more general examination of overall classifier performance.

To select a reasonable gouge probability threshold, the precision and recall of the classifier and decision function as a function of gouge probability are examined. Figure 2 shows the results of computing both precision and recall for various gouge probability thresholds in the decision function. A threshold of 0.3 provides reasonable classifier precision of around 80% for all types while maintaining a recall of over 95% for gouges.

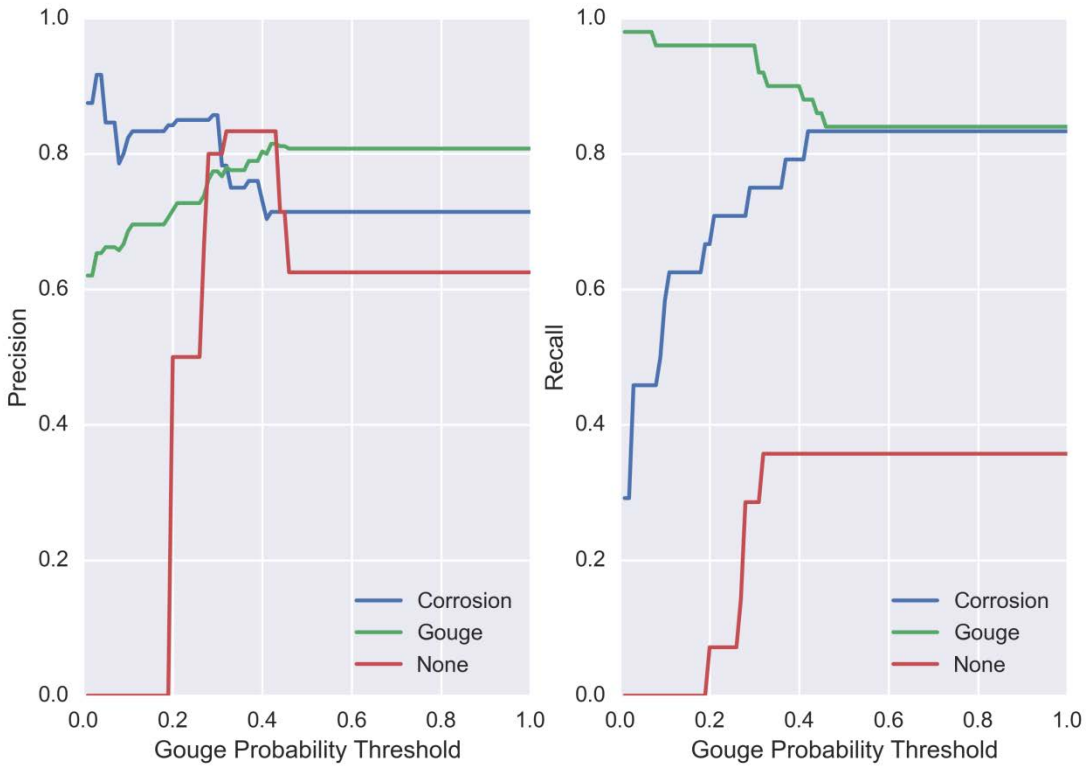


**Figure 2. Precision and recall for the three metal loss types as a function of gouge probability threshold**

Summary details on the number of correctly classified features can be obtained by examining the classifier confusion matrix as presented in Table 2. Table 3 shows a summary of precision and recall for the classifier and decision function combination.

**Table 2. Classifier confusion matrix**

| | Called "Corrosion" | Called "Gouge" | Called "None" |
|---|---|---|---|
| **Is "Corrosion"** | 18 | 6 | 0 |
| **Is "Gouge"** | 1 | 48 | 1 |
| **Is "None"** | 2 | 8 | 4 |

**Table 3. Classifier performance summary**

| | Precision | Recall | Samples |
|---|---|---|---|
| **"Corrosion"** | 0.86 | 0.75 | 24 |
| **"Gouge"** | 0.77 | 0.96 | 50 |
| **"None"** | 0.80 | 0.29 | 14 |
| **average / total** | 0.80 | 0.80 | 88 |

In summary, a random forest classifier that can distinguish dent with gouge from dent with corrosion was developed. A custom decision function was developed that provides a means to vary the conservatism of the classifier so that high recall on gouges can be achieved. A gouge probability threshold of 0.3 achieves better than 95% recall for OOB samples. The details are shown in the table in Attachment A

**Metal Loss Sizing.** Field measurements of metal loss depth were available for 70 of the samples in this study. One of those samples (anomaly ID 90) in the ILI data had no detectable metal loss. Eliminating that leaves 69 samples where both ILI and field metal loss depths can be compared.

For this study, the field measured depth of metal loss anomalies associated with both corrosion and gouge features show that all but four are below 20% depth. One outlier at 58% depth was associated with a very sharp puncture-like feature at Anomaly ID 50. Rather than attempt to fit a specific metal loss sizing model for shallow metal loss associated with dents over such a small range of anomaly size, we instead provide guidance on the best practice to apply existing sizing models. Historically, axial MFL was the primary data set used to size all metal loss. With a full MDS data set, the spiral MFL (SMFL) data is also available for sizing and can be used when appropriate. Best practice is as follows:

- Size the metal loss using the data set where the metal loss signal is most pronounced. For circumferentially oriented features this will be axial MFL. For axially oriented features, this will be spiral MFL.
- The MFL or SMFL response due to the dent geometry itself must be removed from the signature before sizing the metal loss. This is generally obvious as the dent response is slow and gradual across the dent shape whereas the metal loss response is more rapid and local. The dent response in these data sets is largely due to the sensors changing position radially with respect to the magnetizer body. Strong field gradients exist between the field in the pipe wall and the field in the return path in the magnetizer body.

Figure 3 shows the results of applying these practices to the metal loss anomalies in this study. Of the 69 sized features, 56 (or 81%) show agreement between ILI and field measurements within ±10%. A small ILI under call bias of 2% on average exists which is likely due to the very small length and width of some of the metal loss. This level of performance is roughly in line with metal loss sizing performance in the absence of a dent for anomalies of similar size and shape.

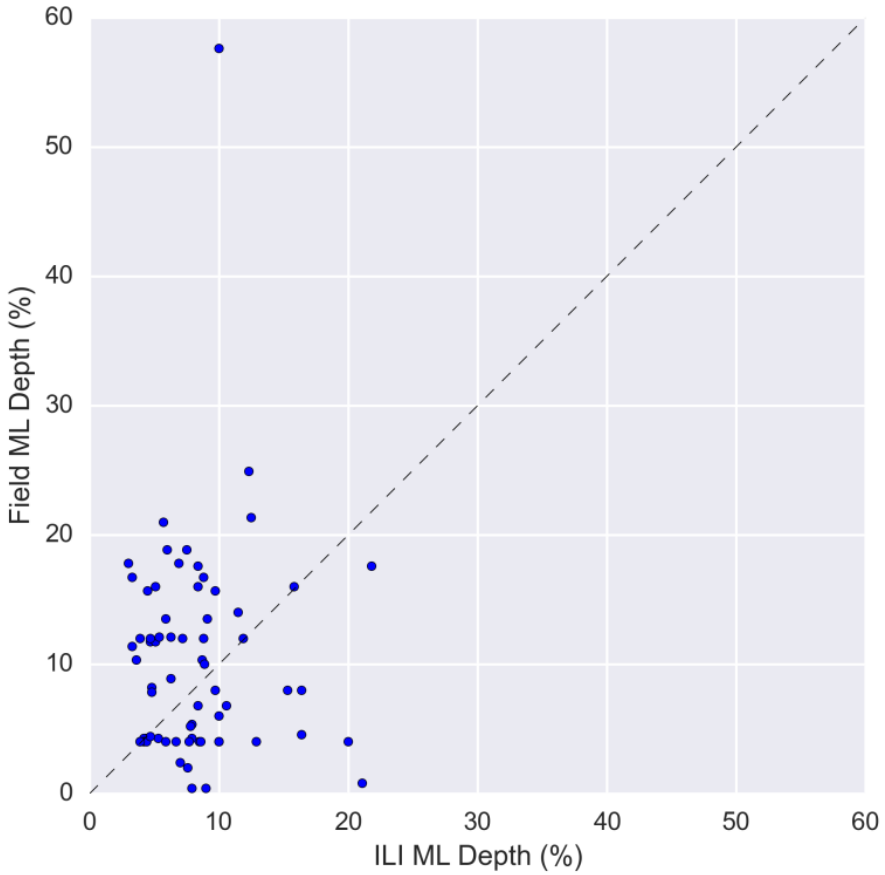


**Figure 3. Metal loss sizing performance for anomalies in dents**

**Summary of Mechanical Damage Classifier.** A random forest classifier has been developed that can distinguish dent with gouge from dent with corrosion. A custom decision function was developed that provides a means to vary the conservatism of the classifier so that high recall on gouges can be achieved. A gouge probability threshold of 0.3 achieves better than 95% recall for OOB samples. Guidelines for sizing metal loss in dents using data MFL and SMFL are provided with produce metal loss depth agreement between ILI and field in dented pipe comparable to that achieved in clean pipe.

## Algorithm for SSWC Discrimination

Historically many ILI vendors have employed a process for identifying potential SSWC based largely on the scrutiny of a subject matter expert (SME). The objective of the current classifier model development is to arrive at a quantitative model that resembles the process that a SME would follow. While there are many forms that such a classifier can take, one of the most commonly used models is logistic regression. It is especially appropriate where the training data set is relatively small and can be separated by a linear decision boundary.

In logistic regression, a linear combination of continuous input variables, often called “features,” is mapped to a continuous output value between 0.0 and 1.0 using the logistic function. It is commonly employed when the goal is to place candidates into one of two classes, the first corresponding to a model output of 0.0, and the second corresponding to 1.0. As such, the output of such a model can be treated as a probability. The continuous probability can be interpreted as the likelihood that the candidate anomaly belongs to the second class. The decision to label each observation as one class or the other is set by selecting a probability level as the decision boundary, often called the discrimination threshold. This is commonly set at 0.5, but it can be set differently to emphasize either false positive or false negative rates [15].

The features selected for input in this study mirror those used by subject matter experts in their qualitative classification. Qualitatively, a large SMFL amplitude response that is sharp in the width (circumferential) direction is an indicator of narrow, axial character to the anomaly. Furthermore, if the SMFL signal response is uncharacteristically large relative to the corresponding MFL response at the same location, then the anomaly is more likely to be SSWC rather than corrosion along the long seam. Accordingly, the input features selected for development of the classifier were signal widths and signal amplitudes from both the SMFL and MFL signatures. Commercial ILI analysis software is used to extract the best estimates of signal widths and signal amplitudes for each anomaly.

Kiefner selected the line segments to target for field activities related to SSWC after TDW had provided a preliminary prioritization of anomalies most likely to be SSWC. A full list of the 39 anomalies used for model development is included in Attachment B Table B1. Note that each anomaly has been labeled as either SSWC or corrosion crossing the long seam (CCLS). Because the number of anomalies available for model development is relatively small a substantial amount of time was dedicated to making sure the correlation between the ILI and field results was accurate. The impact of a single “bad” training example becomes much more important with a small set of data to begin with.

To make the model more general, the raw signal measurements were first nondimensionalized. Signal width and signal amplitude are nondimensionalized by wall thickness and local background flux density, respectively.

$$\begin{aligned} \mathbb{W}_{smfl} &= \frac{w_{smfl}}{t} \quad & \mathbb{A}_{smfl} &= \frac{A_{smfl}}{B_{smfl}} \\ \mathbb{W}_{mfl} &= \frac{w_{mfl}}{t} \quad & \mathbb{A}_{mfl} &= \frac{A_{mfl}}{B_{mfl}} \end{aligned} \tag{3}$$

These four nondimensionalized features are shown plotted as pairs against each other in Figure 4. For the pair plot of the nondimensionalized classifier inputs for the two classes, the red squares represent SSWC, and blue circles represent CCLS. Opportunities for developing a boundary between the two classes are apparent when examining these parameters, especially the signal widths.

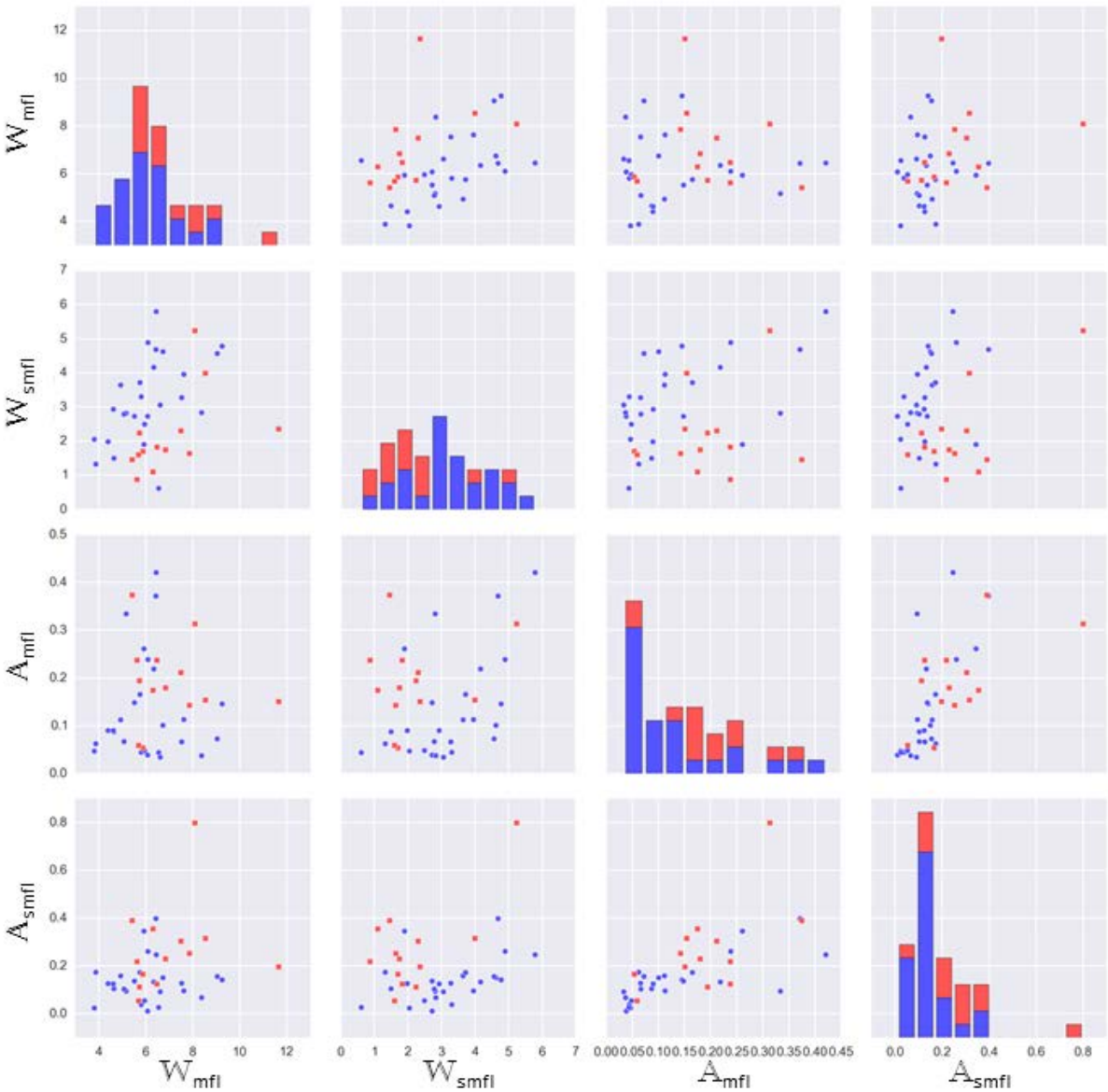


**Figure 4. Pair plot of the nondimensionalized classifier inputs for the two classes. Red squares represent SSWC, and blue circles represent CCLS.**

With input features defined, a logistic regression model of the following form was fit to the full set of 39 training anomalies:

$$F(z) = \frac{1}{1+e^{-z}}$$
$$z = \beta_0 + \beta_1 \mathbb{w}_{mfl} + \beta_2 \mathbb{w}_{smfl} + \beta_3 \mathbb{A}_{mfl} + \beta_4 \mathbb{A}_{smfl} \tag{4}$$

where F(z) represents the likelihood that a particular anomaly is SSWC. Best fit model coefficients are:

$$\begin{aligned} \beta_0 &= -5.21 \\ \beta_1 &= 1.08 \\ \beta_2 &= -1.90 \\ \beta_3 &= 5.42 \\ \beta_4 &= 9.10 \end{aligned} \tag{5}$$

Raw training accuracy is 87% against the original training data using a discrimination threshold of $F(z)$=0.5. Classifier predictions of "probability of SSWC" for all training anomalies are available in Attachment B Table B2. The classifier commits five errors, three of which are false negatives and two of which are false positives.

With a small set of data it is usually necessary to use all of the available data to train the classifier rather than hold out some of the data in a separate model test set. Some form of model cross validation using sets resampled from the training set is pursued instead. For this study, a stratified k-fold cross validation was employed using two folds. A stratified approach preserves the fraction of observations from each class in each fold and also shuffles the observations randomly before dividing the full set into training and test sets. With two folds, half the observations are used to train the model, and then the other half are used to test the model. The process is then repeated with the training and test sets swapping places. Since the process involves random sampling, it is only possible to report representative accuracies on the test sets since rerunning the cross validation exercise produces a different random sample in the two sets. For one representative random sampling, the test accuracies on the two folds were 70% and 79%, somewhat lower than the training accuracy which is to be expected.

Another valuable indicator of model performance is the receiver operating characteristic (ROC). The ROC curve shows the relationship between a classifier's true positive and false positive rates as the discrimination threshold varies from 0.0 to 1.0. The area under the ROC curve is an indicator of overall model performance. An ideal model would have a false positive rate of 0.0 and a true positive rate of 1.0, which would produce an area under the ROC curve of 1.0.

At the other extreme, random assignment of each observation to one of the two classes would have roughly equal false positive and true positive rates, yielding an area under the "random guess" ROC curve of 0.5. A ROC curve was developed for the SSWC classifier model using the same stratified k-fold cross validation split described above. The results are presented in Figure 5.

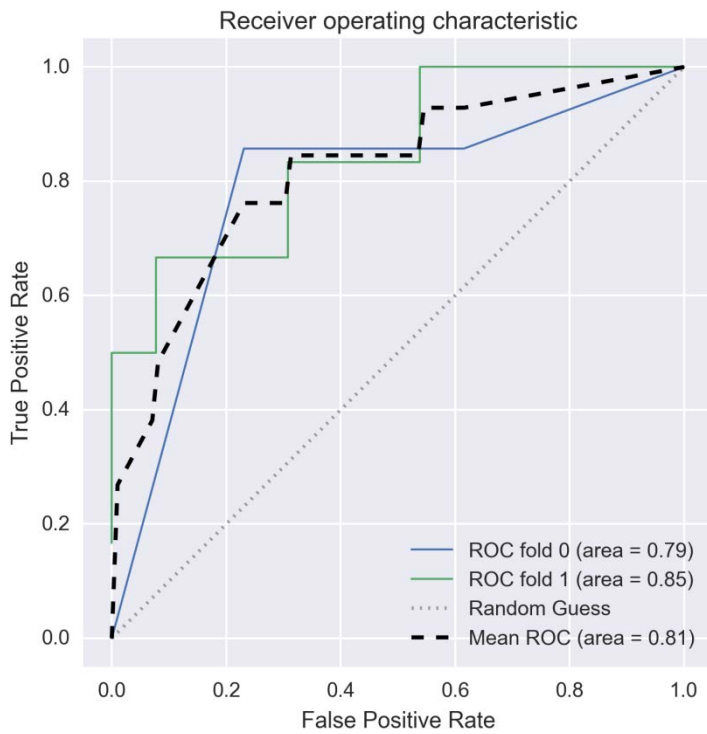


**Figure 5 Receiver operating characteristic for the SSWC classifier**

**SSWC Sizing Models.** Once an anomaly has been identified as SSWC, it is desirable to obtain an estimate of the true anomaly depth and length. Sizing models for conventional corrosion and axial narrow features already exist in TDW's analysis software, but those models do not account for the coincidence of the two. Consequently, adjustments to the standard models are required to appropriately size SSWC.

*Depth Model*. The depth of SSWC is assumed to be a linear combination of the depths obtained from the independent application of the SMFL sizing and MFL sizing models.

$$\hat{d}_{sswc} = \beta_5\, \hat{d}_{smfl} + \beta_6 \hat{d}_{mfl} \tag{6}$$

Training the model on the 13 available SSWC examples yields these coefficients:

$$\begin{aligned} \beta_5 &= 0.68 \\ \beta_6 &= 0.27 \end{aligned} \tag{7}$$

The model performance is shown as a unity plot in Figure 6. No attempt at model validation beyond this graphical approach is attempted here because of the small number of samples and limited depth range available. Model scatter is visually quite small.

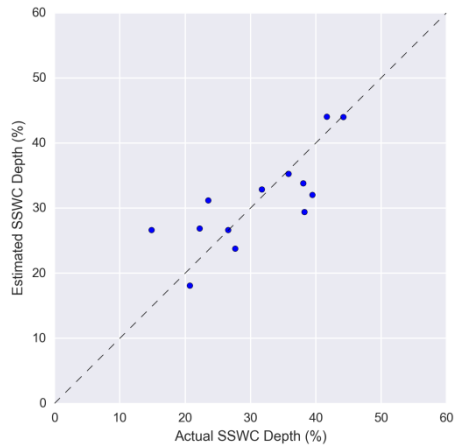


**Figure 6. SSWC depth model performance**

*Length Model.* Similar to the depth model, the length model for SSWC assumes length is a linear combination of the length estimates obtained from the independent SMFL and MFL length models.

$$\hat{l}_{sswc} = \beta_7\, \hat{l}_{smfl} + \beta_8 \hat{l}_{mfl} \tag{8}$$

A best fit to the training data yields these coefficients:

$$\begin{aligned} \beta_7 &= 0.59 \\ \beta_8 &= 0.93 \end{aligned} \tag{9}$$

Model performance is displayed as a unity plot in Figure 7. Model scatter is quite large, most likely due to the ILI tool's inability to detect the shallower extents of an SSWC anomaly whereas very shallow regions of SSWC are often visually apparent under field examination.

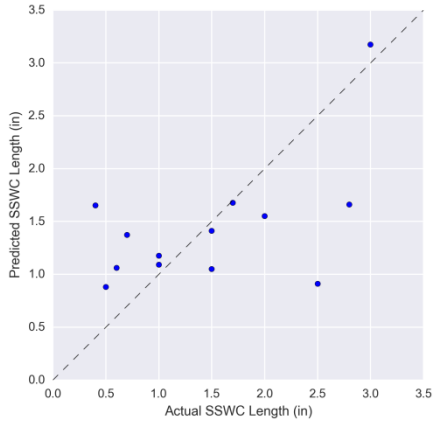


**Figure 7. SSWC length model performance**

**Summary of SSWC Classifier.** A statistical classifier for SSWC has been developed which attempts to quantify the process used by TDW SMEs to identify regions of likely SSWC. The classifier performance has been cross validated using a stratified k-fold approach. Sizing models for SSWC depth and length have been developed and are available for use in prioritizing SSWC locations. Validation of the sizing models was not attempted because of the small number of anomalies available. The depth model shows a much better fit to the training data than the length model.

## Algorithm for Classifying Complex Corrosion

The first step in improving corrosion sizing is developing an improved classifier model for separating complex corrosion inline inspection (ILI) signatures into individual metal loss anomaly calls. The model that has been developed uses ILI data gathered with TDW's Multiple Data Set (MDS) inspection systems. The ILI data originated from actual field use of the systems in operating pipelines with real complex corrosion anomalies. Corresponding field validation measurements were gathered by Applus RTD using high resolution laser scanning systems.

**Data Sources.** TDW has inspected several line segments using MDS ILI systems. The ILI analysis identified some metal loss anomalies that occurred in patterns that would be considered complex and interacting. The project team jointly evaluated which complex corrosion candidate anomalies would be suitable for detailed field examination, and subsequent field evaluation was performed. The final set of anomalies was drawn from the following segments:

- 16" Pipeline D, inspected 2/9/2012
- 20" Pipeline E, inspected 7/11/2013

Laser scanning was performed at two locations in each of the segments, capturing multiple complex corrosion anomalies at each scan location.

**Complex Corrosion Classifier Model.** Magnetic flux leakage (MFL) inspection is an inferential measurement technique in that flux readings are not a direct indicator of the underlying metal loss depth. Instead, the MFL signal patterns must be processed through some set of models to arrive at estimates of anomaly dimensions. The process of sizing complex corrosion signatures is currently a two-step process. First, the complex signature must be partitioned into individual metal loss anomalies. Second, the individual metal loss anomalies are sized using appropriate models, usually some form of machine learning regression model that has been trained to accept certain characteristic features of the individual metal loss signatures and return estimates of the underlying anomaly dimensions. The methods described in this report relate to the first step. Improvements in estimated anomaly dimensions will be addressed in later sections.

While machine learning techniques are most appropriate for *sizing* complex corrosion the techniques of computer vision and image processing are better suited for *classifying* complex corrosion into individual metal loss anomalies. The discussion in the following represents a general approach for taking a complex corrosion signature and breaking it down into constituent metal loss anomalies using image processing techniques. There is inherent ambiguity in this process since there is no general set of rules in the industry for how this is to be accomplished even under direct examination of corroded pipe in the ditch. The methods developed below do not attempt to address this inherent ambiguity. Instead, they represent a reasonable approach that can be reduced to practice in production ILI analysis software with moderate effort.

As an overview of the method, consider that magnetic field data collected from different types of sensors are used to construct individual metal loss anomalies, hereafter referred to generically as *pits*, in a complex corrosion patch. Axial MFL data shown in Figure 8(a) is used as the main source for identifying individual pits in a corrosion patch. SpirALL® MFL (SMFL) data shown in Figure 8(b) is used to compensate for the influence of the direction of the magnetic flux on pit size and shape. The laser scan data shown in Figure 8(c) is obtained by excavating the pipe region where corrosion is identified and by scanning the surface of the pipe with a laser displacement meter. This laser data acts as *ground truth* for both identifying the deepest points of the individual pits as well as future sizing of the pits done using a combination of MFL and SMFL data sets. The process for applying the method is described below using one of the complex corrosion locations from the project data.

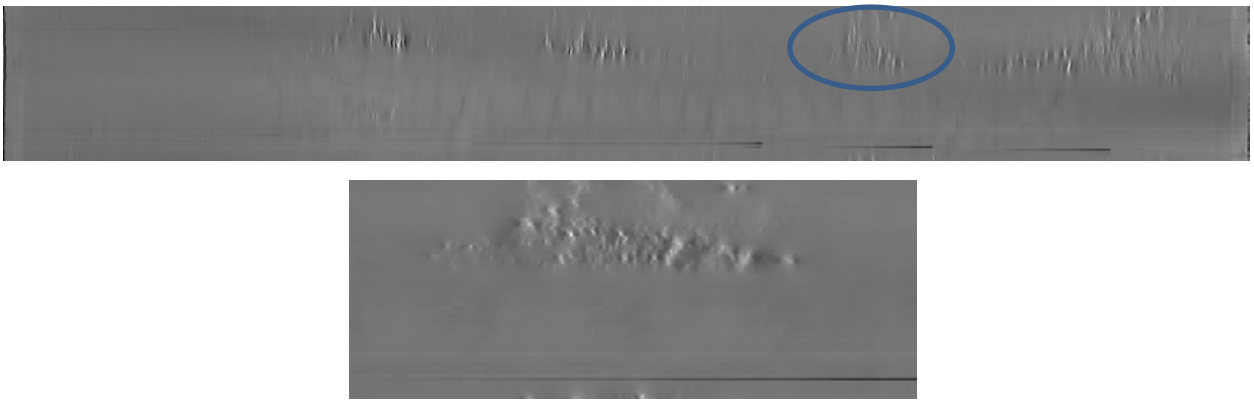

**(a) MFL data of a complex corrosion patch: a small section indicated by circular mark is shown zoomed in.**

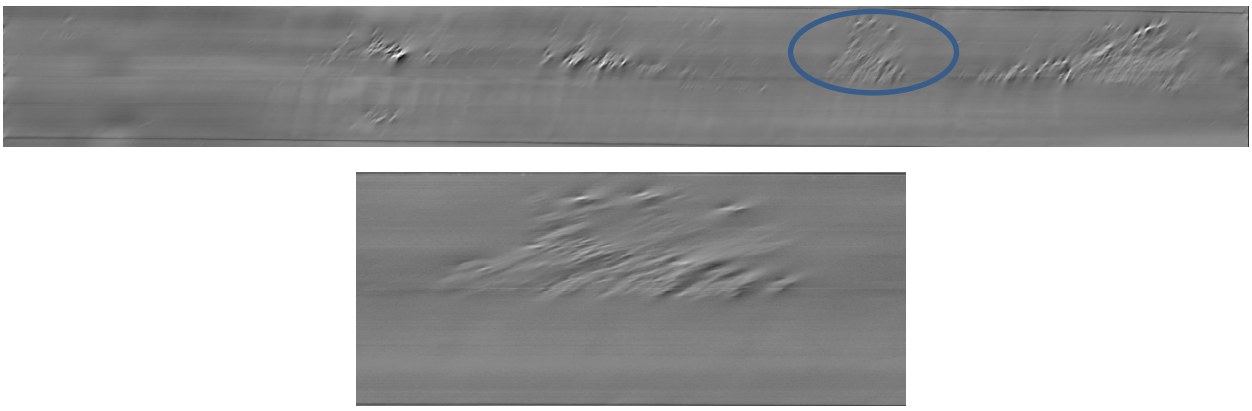

**(b) SMFL data of a complex corrosion patch (same pipe region as above MFL data)**

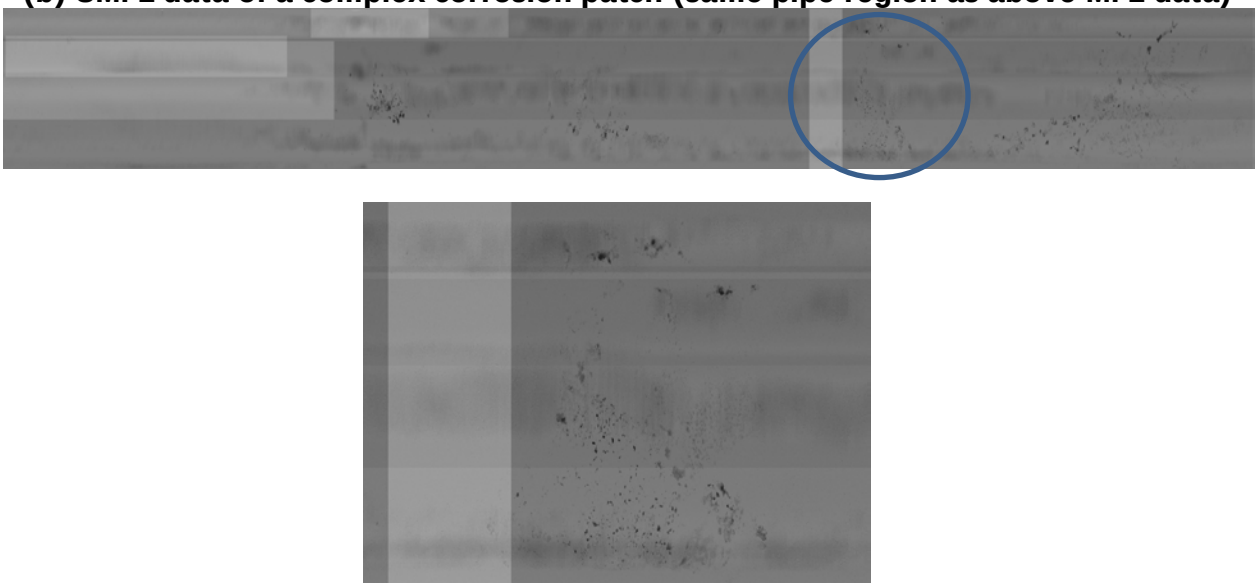

**(c) Corresponding laser scan data of the pipe surface**

**Figure 8. A complex corrosion patch as detected by (a) MFL sensors (b) SMFL sensors and (c) laser scanning of the pipe surface**

*Methodology.* Several data preprocessing and segmentation steps are developed to identify individual pits in a given complex corrosion patch. The end result of processing the data through multiple filters is a list of uniquely labeled pit masks covering the entire complex corrosion patch in MFL data with a corresponding mask in the SMFL data (if a corresponding pit can be uniquely identified in SMFL data). Sizing of the individual pits (and that of a complex corrosion patch) can be accomplished with these masks and checked against corresponding ground truth from the laser scanning data, which will be addressed in later section of this report. Several steps involved in segmentation of individual pits in a complex corrosion patch are listed below.

1. **Remove Tool Rotation.** The MFL and SMFL data are both re-indexed such that first row of the data corresponds to top of the pipe. This is accomplished using the orientation sensor data gathered as part of the ILI inspection log.

2. **Scale and Quantize.** For internal processing purposes the data from the individual sensors is scaled to have a common mean and resampled to 256 quantization values across the total range of observed sensor readings.

3. **Mark Regions of Interest.** The overall rectangular area enclosing the complex corrosion patch is partitioned to identify regions of interest (ROI) in MFL and SMFL data as illustrated in Figure 9. The partitioning is accomplished by an analyst using a graphical user interface that allows for interactive boxing of arbitrarily shaped regions in the MFL data. Both MFL and SMFL data are approximately in sync in the distance domain at this stage, so the resulting marked ROI are applied to both MFL and SMFL data sets.

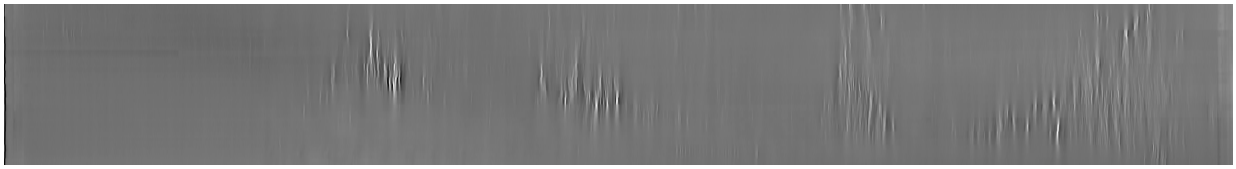

**(a)**

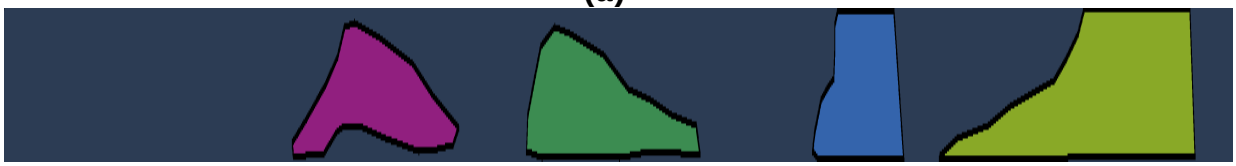

**(b)**

**Figure 9. (a) Part of the MFL data of a whole joint that was later scanned by laser. (b) Interactively marked regions of interest showing complex corrosion patch**

4. **Detect MFL Peaks.** An automated peak detection algorithm searches the MFL data in the ROI for local peaks. Individual peaks in the MFL data are designated in Figure 10 by colored square dots, corresponding to the deepest points in the individual pits; these are signal locations that have shown a magnetic flux leakage above or equal to its neighborhood magnetic flux leakage. Certain statistical criteria are used to reduce noisy peaks.

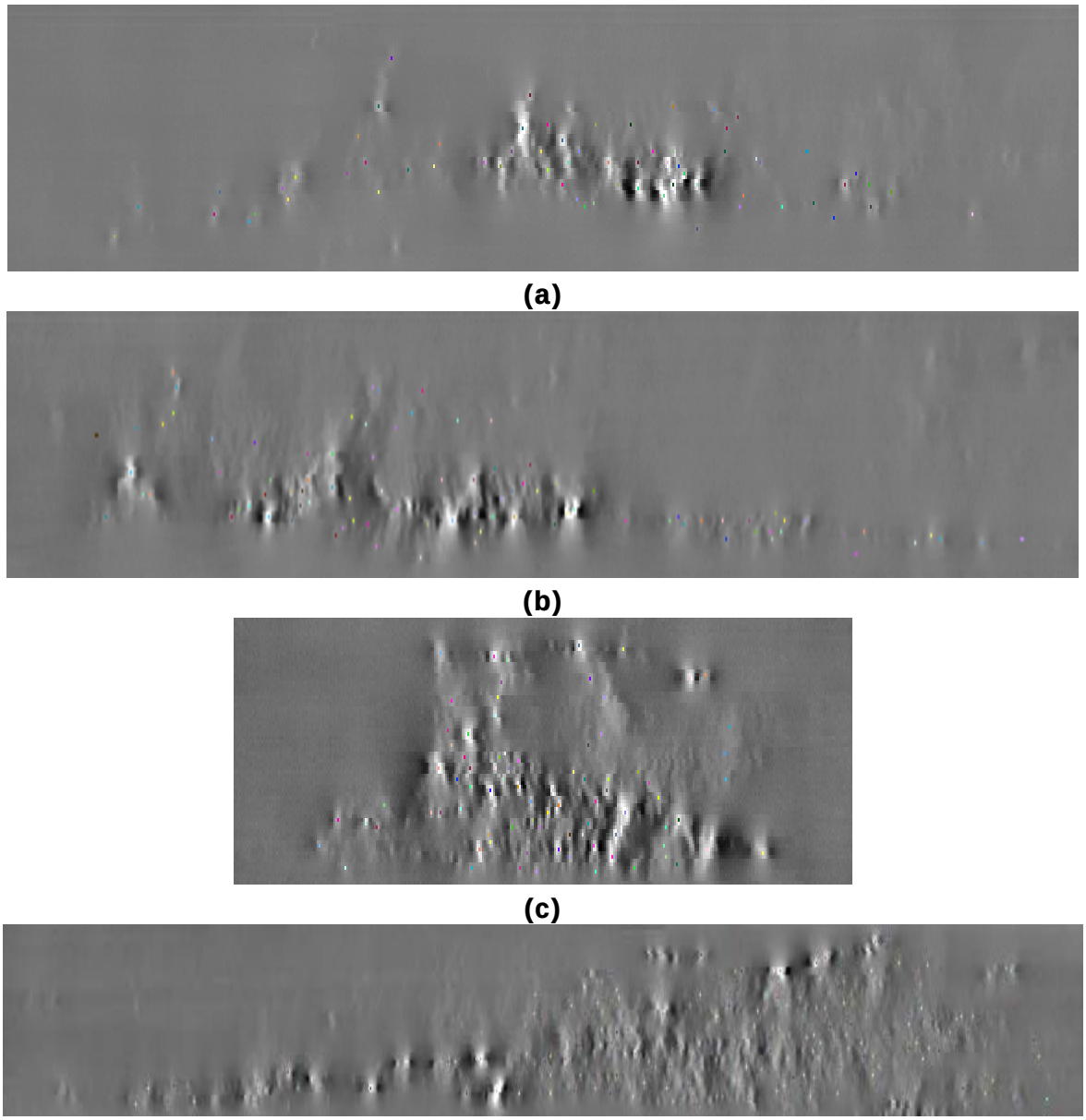


**Figure 10. Four complex corrosion patches in an MFL joint with the peaks of individual pits marked. Colored dots placed on deepest points of the local pits were automatically identified.**

5. **Transfer MFL Peaks to SMFL.** The detected peaks in MFL are registered to the SMFL data by affine transformation as shown in Figure 11. The peak locations are first scaled by a ratio of sensors in SMFL to sensors in MFL data. These peaks form initial peak locations in SMFL. A small window region in the SMFL data around the initial peak is automatically searched for local SMFL peaks. The initial peak is then shifted to the location of highest local SMFL peak within the corresponding region. This local readjustment of the peak position in SMFL while trying to keep the global peak pattern intact can be approximated by a shearing transformation. Conflicts are resolved based on these predefined rules:

    5.1 While undertaking this affine transformation, the peak labels remain constant so that a correspondence between MFL and SMFL peaks is preserved.

    5.2 If there are no corresponding peaks found in SMFL, such peaks are eliminated from the SMFL peak map.

    5.3 If multiple MFL peaks point to the same SMFL peak, the highest and nearest MFL peak will be assigned to the corresponding SMFL peak. The rest of the MFL peaks are eliminated (if they do not correspond to other SMFL peaks) from the SMFL peak map.

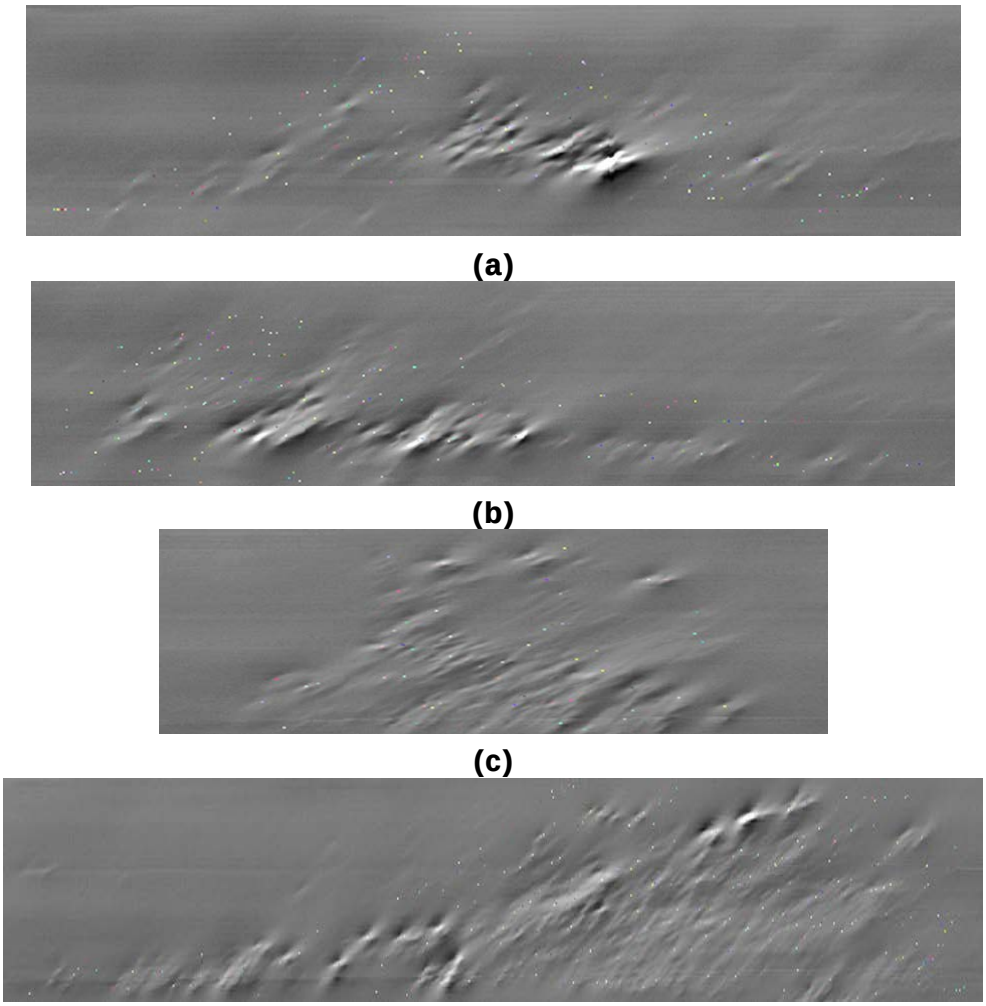


**Figure 11. Peaks identified in the complex corrosion patches of MFL data are mapped onto SMFL data with corresponding scaling, translation and local window search**

**Grow MFL Peaks Into Pits.** After the peaks are identified, they are grown into their immediate neighborhood constrained by the local magnetic flux intensity profile as shown in Figure 12. The region growing process starts from the highest peak.

5.4 If $I_{max}$ is the highest peak value in a given corrosion patch, then this peak is grown into its neighborhood pixels that have a magnetic flux value above or equal to $I_{\max-t}$ where $t$ is the iteration index, and $I_{\max-t} > I_{base}$ where $I_{base}$ is the baseline value corresponding to the clean pipe surface.

5.5 $I_{base}$ can be considered as the average magnetic flux outside of the corrosion patch calculated using ordered statistics.

5.6 After each iteration, the list of peaks is scanned to identify those peaks that are equal to or above $I_{\max - t}$. If any such peaks are found, those peaks will be added to the list of peaks that are actively growing into their immediate neighborhood. The growth of an individual peak is terminated if there are no pixels in the neighborhood into which the peak region can grow into, under given constraints.

5.7 The iterative region growing is terminated when all the peaks have stopped growing. If there are 'p' peaks and $\mathrm{R}_{\mathrm{j}}^{\mathrm{t}}$ is the total region grown by the peak 'j' at the end of iteration 't', then the region growing is stopped if,

$$\sum_{j=1}^{p} R_j^{t-1} = \sum_{j=1}^{p} R_j^{t}$$

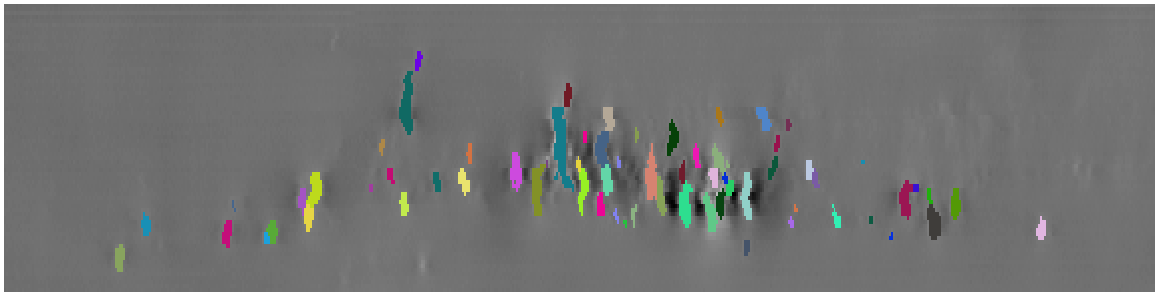

**(a)**

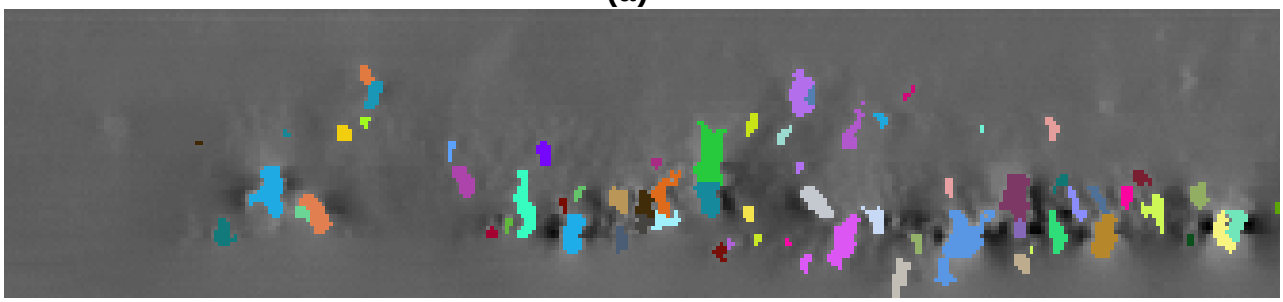

**(b)**

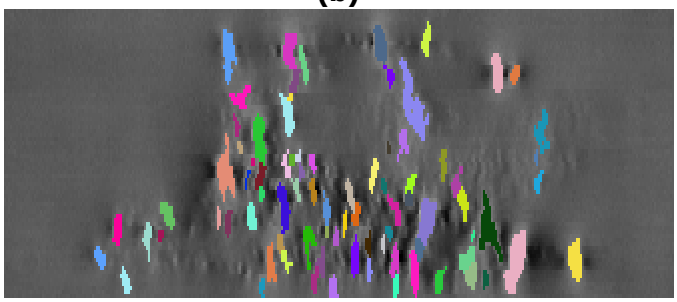

**(c)**

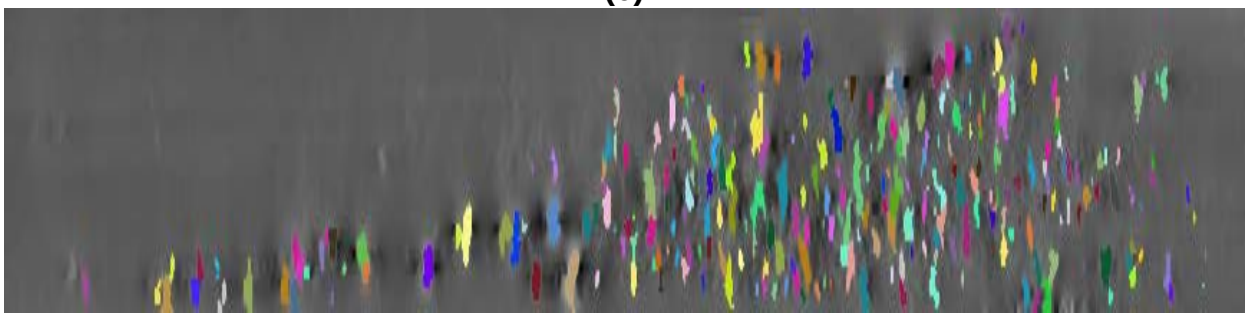

**(d)**

**Figure 12. The MFL pits segmentation by a constrained region growing method in the four complex corrosion patches of the MFL data**

6. **Grow Corresponding SMFL Peaks into Pits.** The corresponding peaks in the SMFL data are also grown into respective pits using the same region growing algorithm, shown in Figure 13.

**(a)**

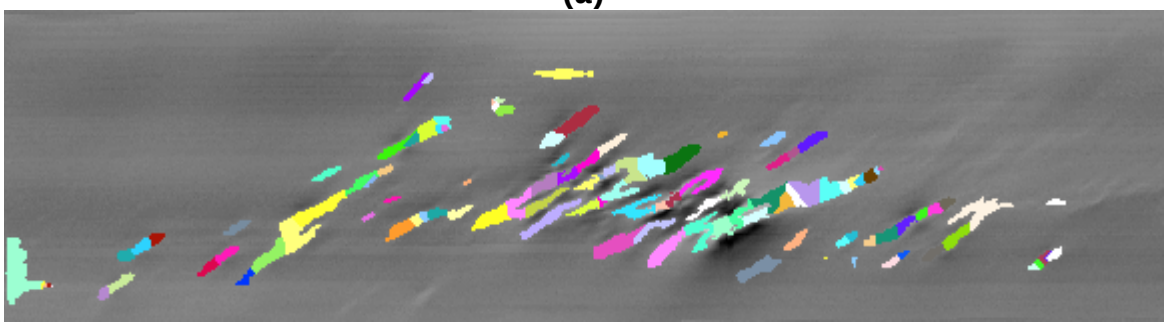

**(b)**

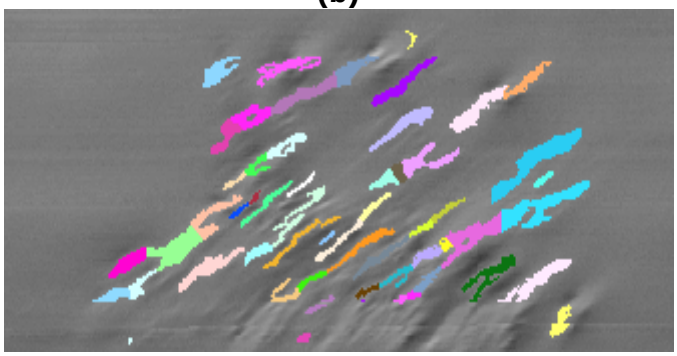

**(c)**

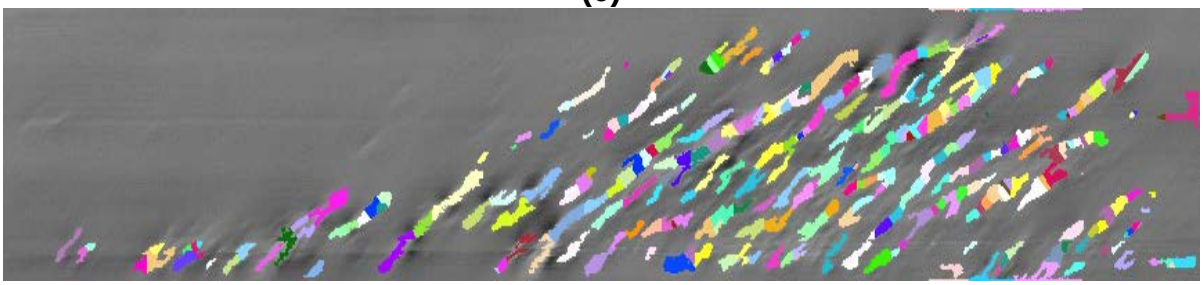

**(d)**

**Figure 13. Result of individual pit segmentation in SMFL data. Each pit has a direct correspondence with pits in MFL. Pits in SMFL have a corresponding pit in MFL with a same label.**

**Model Verification.** The laser scan data are used as ground truth for verification of the pit segmentation in MFL data as well as to facilitate the future sizing of the pits. The process of registering MFL data to laser data is more challenging. This process involves the following steps:

1. **Correct for Scan Direction.** Generally, laser data does not cover the complete joint either axially or circumferentially. Both the starting location and the circumferential scan area (including the direction of scan) are passed as input information to the MFL region extracting method. The MFL data region thus extracted would match the same pipe region from which laser data were scanned.

2. **Approximate Synchronization.** In the second step, the laser data is synced to the MFL data in the axial direction using reported ILI distances and recorded field records taken in the ditch. Since a small scaling discrepancy between the MFL axial distance and the laser axial distance is inevitable this initial synchronization will only be approximate.

3. **Down Sample Laser Data for Automated Final Synchronization.** Laser data are resized to the same number of rows as MFL data, i.e. converted to lower resolution data, for use in an automated synchronization algorithm.

4. **Scale, Quantize, and Automatically Synchronize.** Both regional MFL data and laser scan data are then preprocessed to have common mean across their rows and scaled to equal number of quantization levels, e.g., 256. The two data are then automatically synchronized using cross-correlation within a limited translation, rotation and scaling window.

5. **Transfer MFL Peaks to Down-Sampled Laser Data.** After the laser data and MFL region data are appropriately synched the MFL peaks are superimposed onto laser data as in Figure 14. Using a method similar to the one where MFL peaks are superimposed on SMFL data, we locally adjust the initial peak position to correspond to a local peak position by applying local shearing (non-linear shift). Every peak in MFL is expected to have a corresponding peak in the laser data and hence no peak is eliminated in this process.

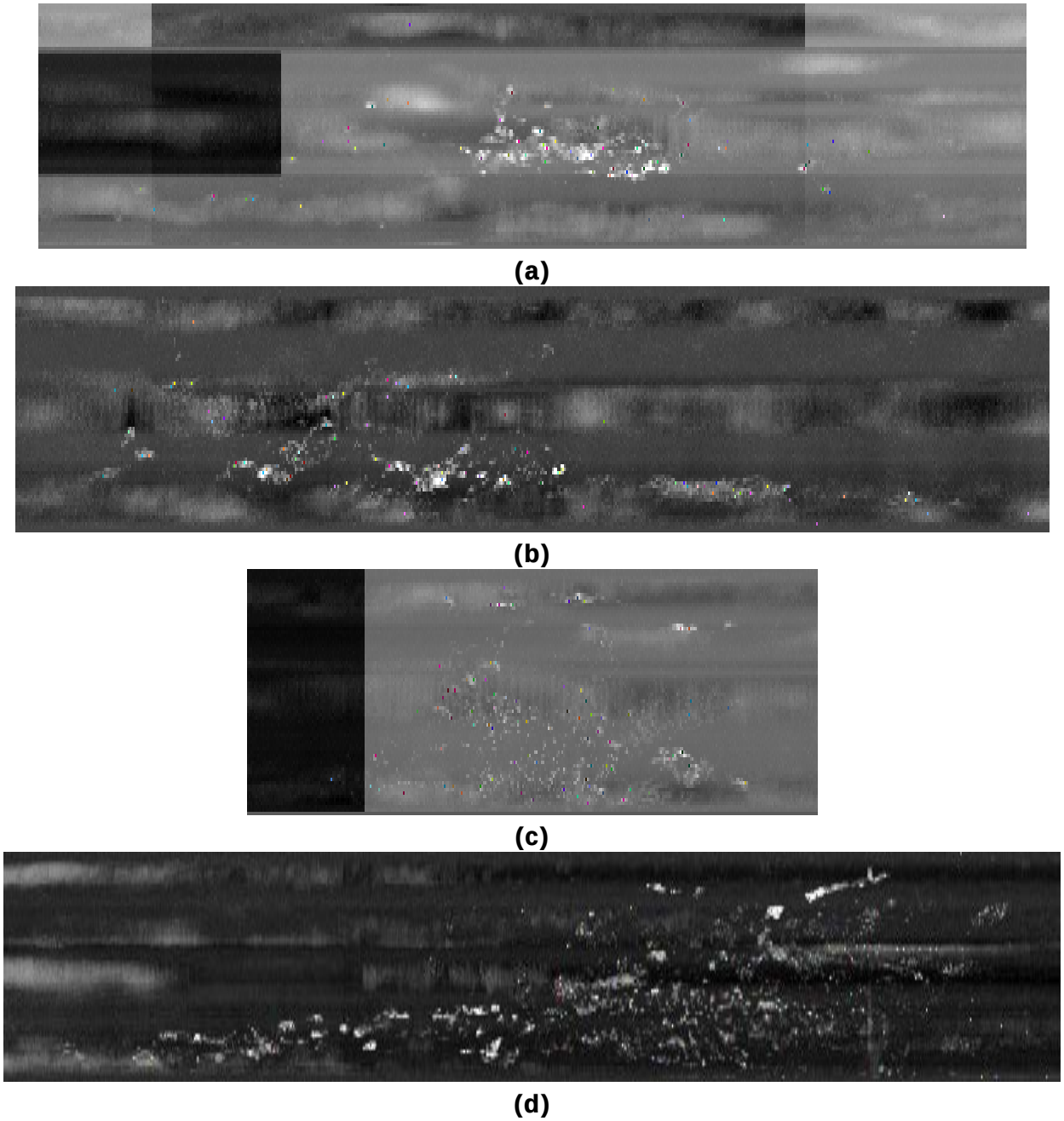

**(a)**

**(b)**

**(c)**

**(d)**

**Figure 14. The peaks of MFL are mapped to low resolution laser data of complex corrosion patches.**

6. **Transfer Peaks to Full Resolution Laser Data.** Peaks are then mapped back onto full resolution laser data as in Figure 15.

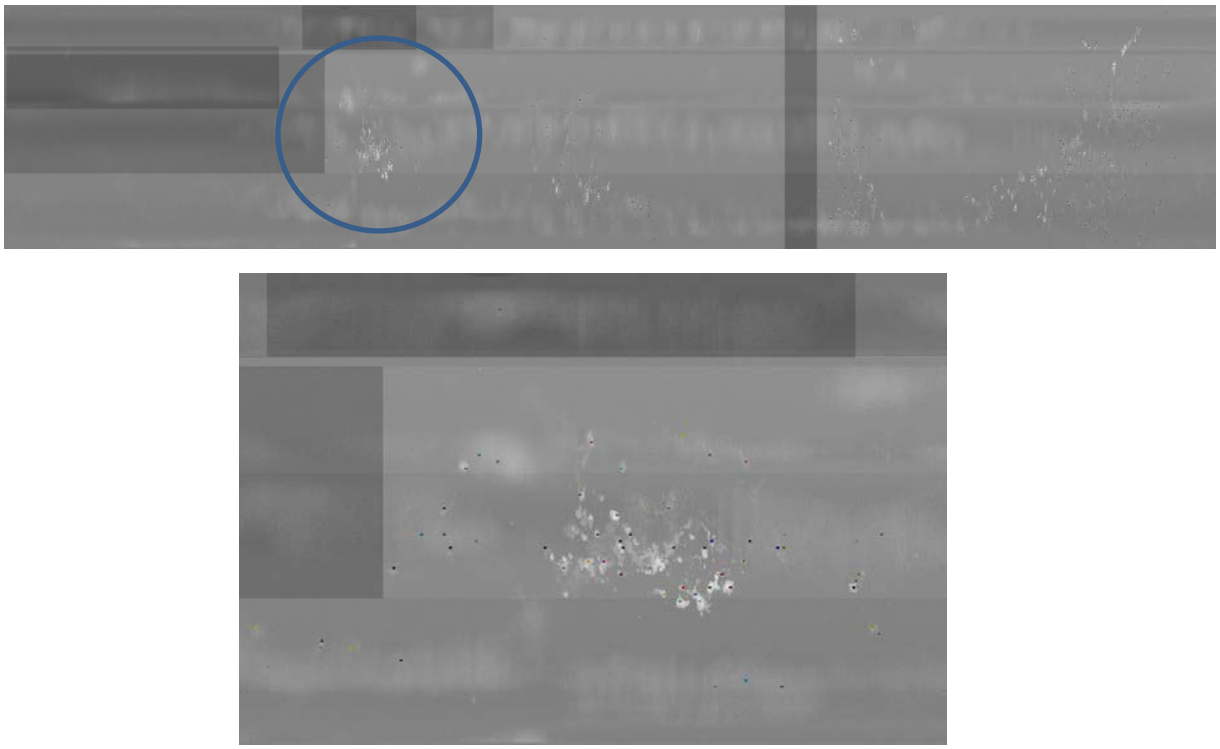

**Figure 15. Peaks marked on full resolution laser data of the complex corrosion patches**

7. **Grow Peaks in Full Resolution Laser Data.** Peaks in the laser data are grown using a similar region growing algorithm used for MFL and SMFL pit segmentation as shown in Figure 16. It is apparent that many smaller pits in the laser data are not separately identified in the MFL data. Also, there are some erroneous regions grown as pits in the laser data due to stitching artifacts in the laser data at boundaries between scans. These may require manual removal.

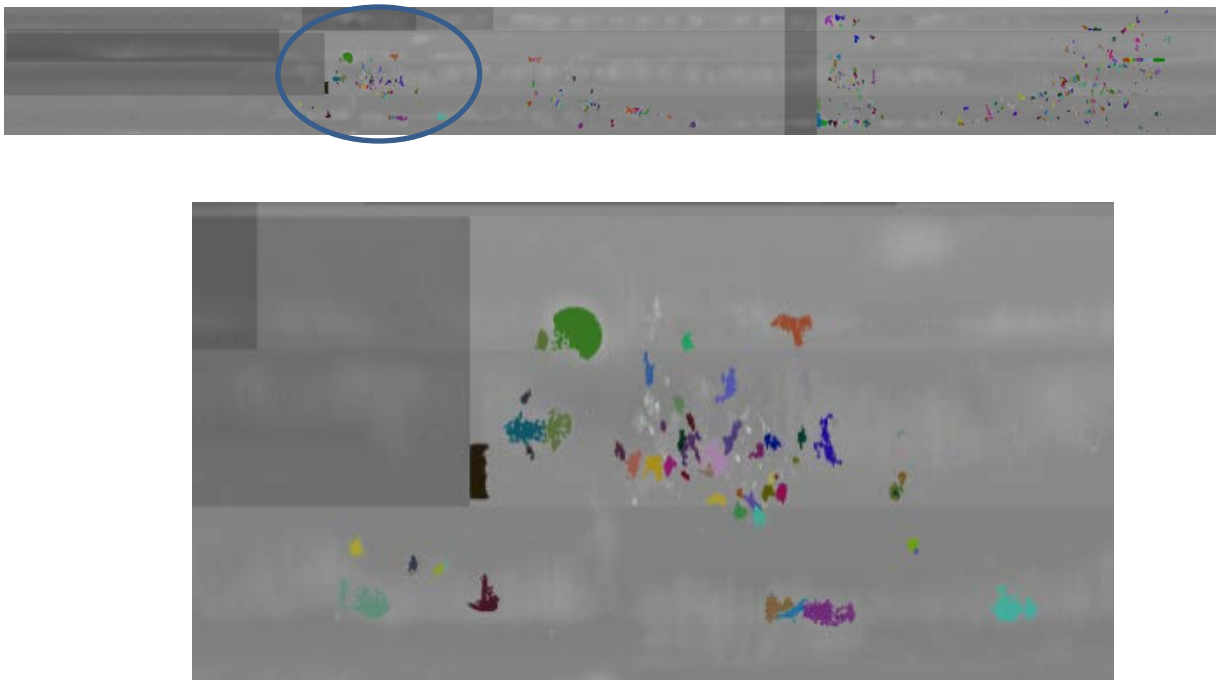

**Figure 16. The pits segmented in laser data using the pits identified in MFL data. Many pits in the laser data have gone unmarked (white areas) as those pits are either not identified in MFL data or merged with other pits in the lower resolution MFL data.**

**Summary and Recommendations on Corrosion Classifier.** A classifier for segmenting complex corrosion patches into individual metal loss anomalies or pits has been developed using image processing techniques. At this stage each individual pit region as identified in the MFL data is marked by a uniquely labeled mask. Most of these pits have corresponding masks in SMFL data and a definite mask representation in the laser data. The data in the masked regions of ILI data will form the input features to a new sizing model. The data in the masked regions of the laser data will serve as ground truth for training that model which will be developed in the next phase of the project.

The segmentation procedure presented here is suitable for corrosion that produces at least moderate signal response in axial MFL data. This will be the most common case for complex corrosion patches. However, for narrow, axially-oriented corrosion axial MFL produces very little response, and the SMFL signal response alone would be more appropriately used to assess these areas. A future improvement to the procedure could be developed that seeks to identify unique signal peaks that exist only in the SMFL data and uses those unique peaks to define pit and axially elongated regions, although it is not clear what the specific decision rules should be to flag certain SMFL peaks as unique rather than associated with a neighboring MFL peak.

## Algorithm for Sizing Complex Corrosion

The second step is to develop an improved sizing model for complex corrosion inline inspection (ILI) signatures. This model has been developed using ILI data gathered with TDW's Multiple Data Set (MDS) inspection systems. The ILI data originated from actual field use of the systems in operating pipelines with real complex corrosion anomalies. Corresponding field validation measurements were gathered by Applus RTD using high resolution laser scanning systems.

TDW has inspected several line segments using MDS ILI systems. The ILI analysis identified some metal loss anomalies that occurred in patterns that would be considered complex and interacting. The project team jointly evaluated which complex corrosion candidate anomalies would be suitable for detailed field examination, and subsequent field evaluation was undertaken. The final set of anomalies was drawn from the following segments:

- 16" Pipeline D, inspected 2/9/2012
- 20" Pipeline E, inspected 7/11/2013

Laser scanning was performed at two locations in each of the segments, capturing multiple complex corrosion anomalies at each scan location.

**Background.** Magnetic flux leakage (MFL) inspection is a well-established, mature technique that has been successfully applied to pipelines for many years now. Nevertheless, MFL users are still faced with limitations to the technology that can be roughly categorized into three areas. These limitations become particularly apparent when dealing with complex corrosion patches.

First, unlike ultrasonic inspection techniques (UT) which return direct measurements of remaining pipe wall, MFL is an inferential technique that uses a mathematical model to translate signal responses into measurements of essential dimensions of corrosion geometry. The physics of the technology make it impractical to formulate an MFL model that can return a uniformly spaced grid of depth measurements across a section of pipe surface in a similar fashion to UT. Instead, an MFL model is generally trained to estimate the essential dimensions of length, width, and depth for a distinct corrosion pit that happens to coincide with a recognizable distinct peak in the MFL signature. When corrosion becomes highly interactive and complex, the identification of distinct corrosion pits in the complex patch becomes quite challenging. Neighboring anomalies can influence the signal acquired which significantly complicates the analysis methodology. This represents one possible approach to the problem of partitioning complex corrosion patches. More importantly, there is no standard procedure today for establishing *truth* for the essential dimensions of length, width, and depth for each

distinct corrosion pit in a complex patch. The work presented below presents one simplistic approach to this problem, but this question deserves more attention elsewhere.

Second, it is not immediately obvious which *features* of the MFL signal directly correlate to the essential dimensions of the underlying corrosion pits. This is particularly true in the case of complex corrosion as the closely spaced metal loss regions cause the MFL signatures to interact with each other in more complex ways. The selection of candidate features for inclusion into a model is largely a matter of trial and error.

Third, the field process for gathering high quality training data for MFL model development is costly, and consequently the amount of data available for modeling is usually relatively small. Furthermore, the training data is rarely spread evenly across the entire ranges of length, width, and depth over which the model is expected to perform. This is especially true for complex corrosion patches, where the patch is usually dominated by widespread, shallow surface corrosion encompassing isolated deeper pitting anomalies.

As a brief review previous section focused on separating complex ILI signatures into individual metal loss anomaly calls. MFL data shown in Figure 17(a) is used as the main source for identifying individual pits in a corrosion patch. SpirALL® MFL (SMFL) data shown in Figure 17(b) is used to improve the pit sizing accuracy by using pit signature shape variation in a different direction of the magnetic flux. The laser scan data shown in Figure 17(c) is obtained by digging the pipe region where corrosion is identified by MFL data and then scanning the surface of the pipe with a laser displacement sensor. This laser data acts as ground truth for both identifying the deepest points of the individual pits as well as sizing of the pits using a combination of MFL and SMFL data.

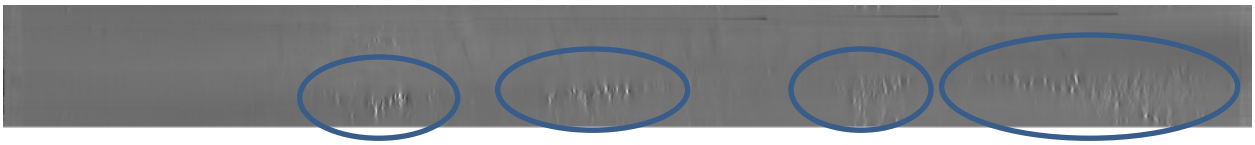

**(a) MFL data of a complex corrosion patch**

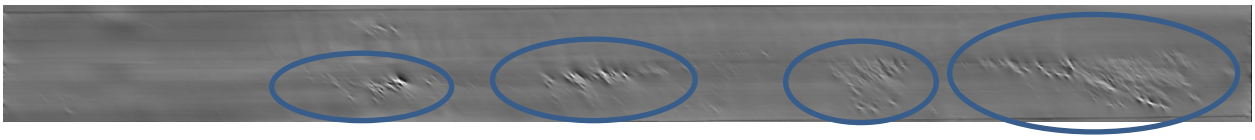

**(b) SMFL data of the same complex corrosion patch**

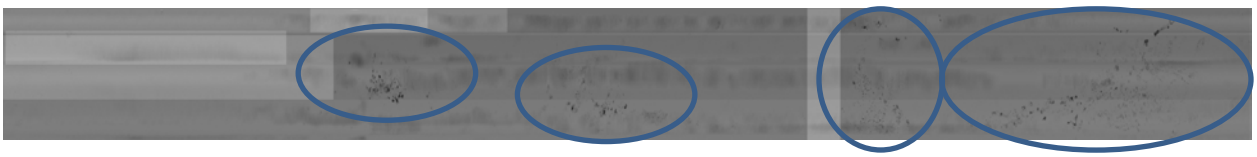

**(c) Corresponding laser scan data of the pipe surface (ground truth data)**

**Figure 17. A complex corrosion patch as detected by (a) MFL sensors (b) SMFL sensors and (c) laser scanning of the pipe surface**

In the previous section, we described the methods developed to identify, segment, and register individual pits across different sensor data. We have improved some of the methods described in the earlier report, specifically in segmenting the pits in the laser data and matching them to corresponding pits in MFL and SMFL data. For this purpose, the laser data is subjected to a few steps of preprocessing that include background leveling, automated and localized thresholding, component labeling, and morphological filtering. The segmented laser data with uniquely labeled individual pits is shown in Figure 18(a). The MFL image is suitably trimmed and magnified so that it corresponds to the same physical area of the pipe scanned by the laser. The MFL pit signatures are then projected onto the laser data, and all the laser pits that are located within a uniquely labeled MFL pit region are given the same label as the MFL pit. The relabeled laser data, where the labels correspond to MFL pit labels, are shown in Figure 18(b). One of the conclusions here is that the laser data which act as a ground truth has to be collected with much more care and all patch like structures and intensity variations that are not pits should be reduced if not completely eliminated.

It should be emphasized that one of the goals of this approach was to arrive at a semi-automated method for processing these complex corrosion patches. The separation and sizing of complex corrosion patches is currently a time-consuming and tedious process for an ILI analyst. The analyst exercises substantial judgment in the process. Reducing the variability in this human process would be a desirable outcome of this semi-automated approach.

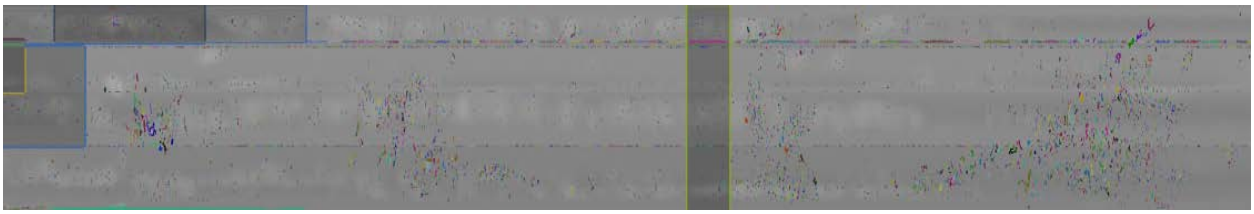

**(a) All pit-like structures in the laser data are segmented and labeled. Even after preprocessing a significant number of noise artifacts can be seen.**

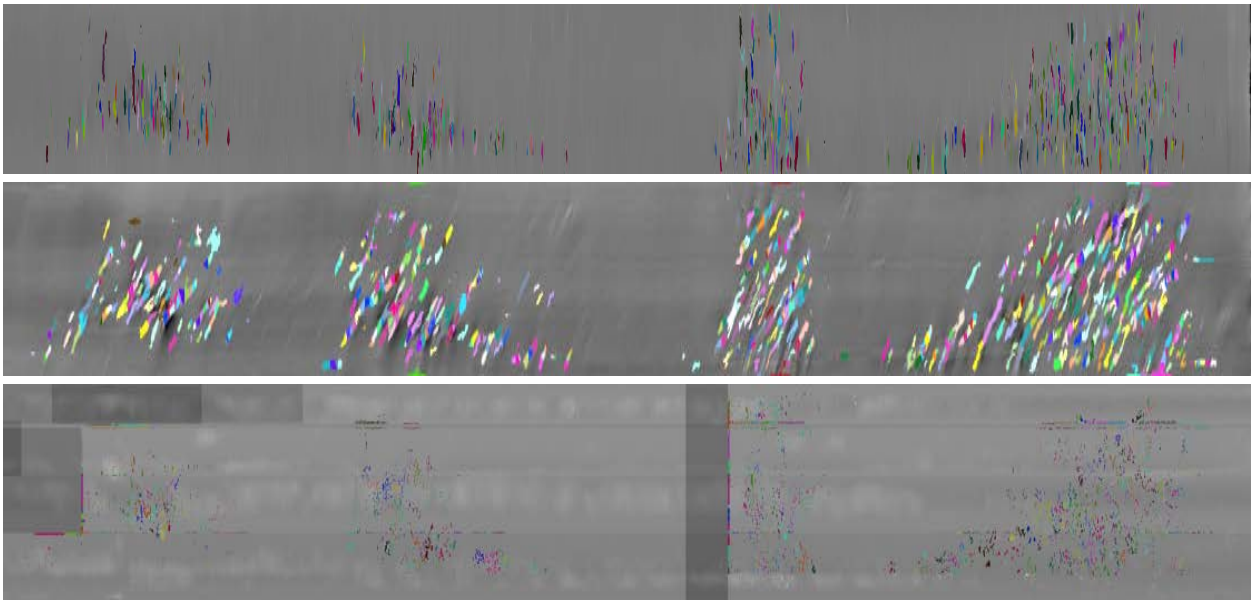

**(b) MFL pit regions, corresponding SMFL pit regions and laser pit regions. MFL pits are matched with the regions in laser data, and the laser pits that are within MFL pit regions are relabeled. Remaining pit objects in laser data are discarded. Colors for the label are randomly selected in each individual image and hence the colors can differ from MFL to SMFL to laser; the recorded labels within the software remain the same across all the images.**

**Figure 18. Labeling and matching ILI pit regions to laser data pit regions**

**Establishing Ground Truth.** Establishing true corrosion size is a critical step in developing an ILI sizing model using machine learning methods. This process is often referred to as establishing ground truth. The laser scan measurements are certainly a very accurate representation of the pipe surface, but the scanner captures many shallow pits which are not distinctly and separately visible in the ILI data. To this end, we developed a process for assigning axial length, circumferential width, and wall loss depth to a collection of laser pits that coincide with an MFL pit. Figure 19 shows a segmented complex corrosion patch where multiple laser pits that correspond to an individual pit in the MFL data are given. All adjacent laser pits that correspond to a single MFL pit are assigned the same color.

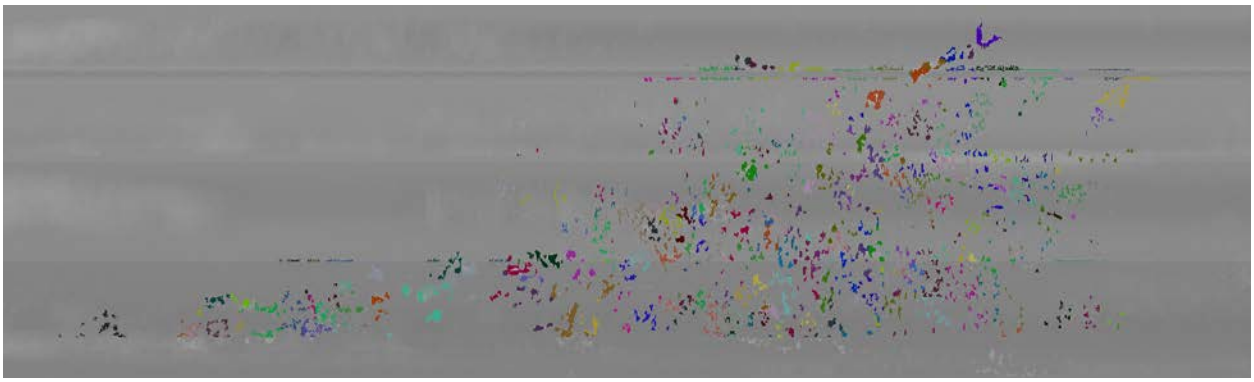

**Figure 19. A complex corrosion patch in the laser data segmented and labeled to match corresponding pits in the MFL data**

For each collection of laser pits of the same color, the following rules are applied to establish ground truth:

- True length is defined as the axial extents of the collection of laser pits.
- True width is defined as the circumferential extents of the collection.
- True depth is defined as the deepest point in the collection.

The application of these rules results in a total of 630 truth samples to be used for model training. As illustrated in Figure 20, the distribution of ground truth is highly skewed toward shallow corrosion features with only a handful of deep corrosion pits in the data set. An ideal data set would show a uniform distribution across the desired modeling space. In practice this ideal is very difficult to obtain from naturally occurring corrosion, and hence most modeling exercises utilize artificial anomaly sets. On the other hand, it is very difficult to create meaningful artificial anomaly sets that exhibit the type of complex interaction that is the target of this work.

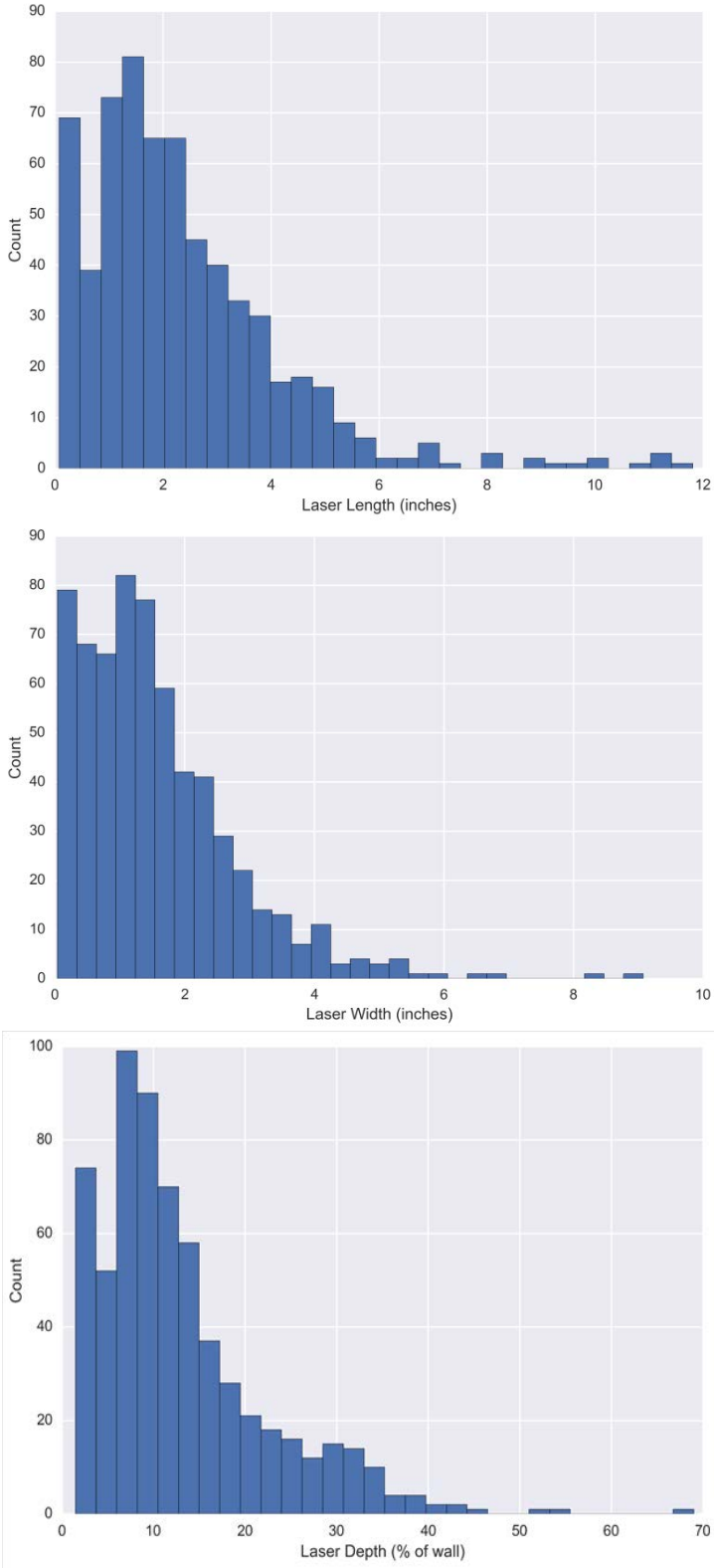


**Figure 20. Approximate distribution of ground truth measurements from laser data**

**Feature Engineering**. As a significant portion of time toward the current project was dedicated to identifying relevant features in the various ILI signatures, developing methods to measure these features, and exploring possible relationships between pit features in the magnetic field data, and the corresponding ground truth from the laser data. Current sizing models estimate the length, width, and depth of a corrosion feature as a function of a handful of ILI signal geometric characteristics and magnetic field strength measurements. For this work, we investigated the inclusion of many additional ILI signal characteristics as features in the sizing model. A description of these new features is provided below.

- Average signal amplitude: The average value of the flux leakage signal, with respect to background level, across the signature.
- Average signal amplitude above half: The average value of the flux signal with respect to background level for that portion of the signal above half the peak amplitude.
- Plan surface area: The area of pipe surface covered by the ILI signature.
- Volume: An approximate volume of the ILI signature where area is length units as obtained above, and the remaining height unit is in gauss.
- Best fit ellipsoid radii: The three radii of the ellipsoid that best fits the ILI signature.
- Best fit ellipsoid orientation: The orientation of the ellipsoid major axis with respect to pipe centerline.
- Best fit ellipsoid volume: Volume of the fit ellipsoid.
- Best fit ellipsoid surface area: Surface area of the fit ellipsoid.
- Shape eccentricity: Ratio of the shortest distance between pit centroid and pit surface to the longest distance between pit centroid and pit surface.
- Center of gravity distance difference: The distance between the rigid body centroid and magnetic field weighted centroid of the signature.

Again the focus was on features which could be extracted in a semi-automatic fashion without the intervention of an analyst. Each of these features was extracted from both the MFL and SMFL signatures that correspond to each of the 630 training samples.

**Model Development.** For this effort, we elected to use Kernel Ridge Regression as the as basic model topology (Murphy). A complete discussion of machine learning and model selection is beyond the scope of the effort here, but we highlight a few of the reasons for selecting this model topology:

- Ridge regression provides for a convenient method for regularization to control for over fitting.
- The provision of kernel selection provides a means to control the inherent nonlinearity and hence the flexibility of the basic model.

- The algorithm is widely available in various, stable software implementations (Pedregosa).

We pursued two approaches to model fitting. In the first, we selected a very flexible model topology and minimal regularization at the risk of over fitting the training results. We did this to examine whether this model topology had enough basic flexibility to reasonably model the nonlinearity of the problem at hand. In the second, we used a k-fold cross validation technique to select the optimal regularization parameters that minimize a cross validation error. This approach should yield a model that is not over fit to the training results and should therefore perform better on new blind samples.

Since we have elected to use all of the data in the training process there is no meaningful way to compute model performance statistics that would translate into performance on new blind samples. We chose instead to provide graphical representations of performance here to provide a qualitative overview of the results.

*Flexible Model.* A polynomial kernel of degree three and regularization parameter of $\mathbf{10^{-10}}$ (essentially zero) were selected for the flexible model. The input features and matching ground truth were fed to the training algorithm, and the original model training data was then re-used to produce predictions of size using the model. The results of those predictions are presented in Figure 21. The model topology is at least flexible enough to predict length, width, and depth with no severe overcall or undercall bias. Scatter in both the length and width models is a bit larger than expected.

We reemphasize that this flexible model is deliberately over fitting the training data. As such, this level of performance would not be expected on new blind samples. The performance of the regularized model below provides a better estimate of performance on new blind samples.

*Regularized Model.* K-fold cross validation was used to select the kernel type, the kernel degree, and the regularization constants. A hyper grid was created across these various model control parameters, and the entire space was exhaustively searched for the combination of parameters that yielded the lowest cross validation error. The best combination of model parameters is different for each of the various predictors:

- Length: polynomial kernel of degree two with regularization constant $\alpha = 10000$.
- Width: linear kernel with regularization constant $\alpha = 10$.
- Depth: radial basis function for the kernel (has a Gaussian shape) with regularization constants $\gamma = 0.1$ and $\alpha = 0.01$.

Figure 22 shows the model performance graphically. The results seem to indicate that the models that produce the lowest cross validation error are essentially predicting a noisy constant.

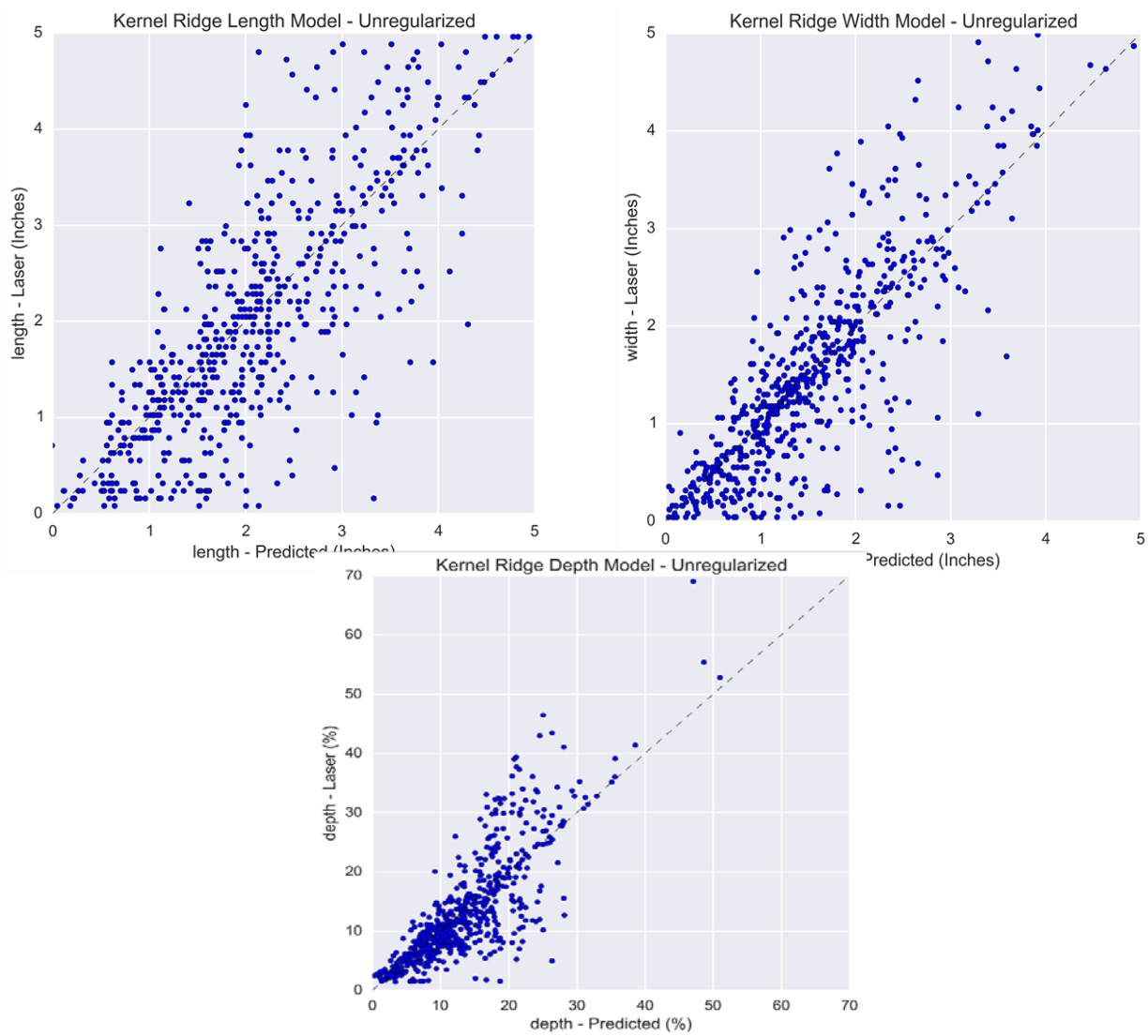


**Figure 21. Unregularized model performance**

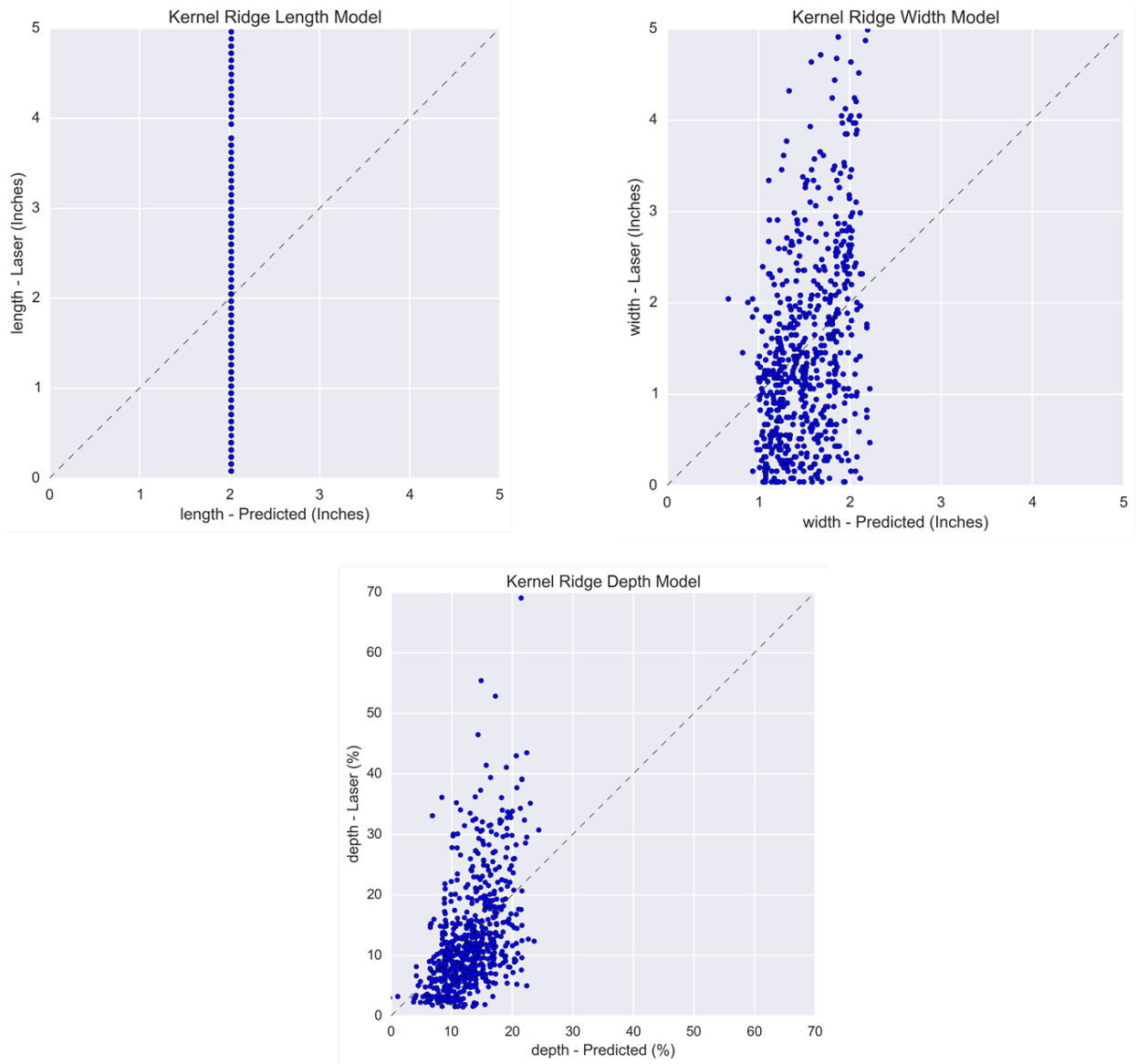


**Figure 22. Regularized model performance**

# VERIFICATION

A conservative approach to verifying the dent with metal loss and SSWC classifiers used pressure testing of the smallest detected anomaly. If the smallest detected anomaly did not fail, then smaller anomalies that have a lower failure pressure would be safe; larger anomalies would be selected for excavation, assessed and repaired as necessary. This approach is inherently conservative as larger anomalies would be identified for repair even though they may pass a pressure test. The corrosion classifier and sizing models did not require burst testing since the assessment standards such as ASME B31G, RSTRNGTH or KAPA provide accepted failure pressures.

For the mechanical damage sample, one dent with a gouge that was identified as a gouge by the classifier was removed from service. The pipe properties were Grade X52, 508mm (20 inch) diameter and 6.35mm (0.250 inch). The dent measured 1.2 percent of the diameter and contained three gouge marks. The pipe was subjected to a pressure test to 100 percent of specified minimum yield stress (SMYS). The pipe did not fail after completing five pressurizations to simulate five hydrostatic tests.

For the SSWC classifier, three pipe samples containing SSWC were removed from service. The pipe with the small SSWC was pressure tested and failed at a pressure of 3,340 psig and did not fail in the longitudinal seam. This pressure exceeded the calculated yield strength pressure of 2,167 psi. It also exceeded the pressure required to reach the pipe flow stress, the average of the yield stress YS and ultimate tensile stress (UTS), (YS+UTS)/2, of 3,259 psig. Therefore, it was concluded that the ILI tool and classifier are capable of identifying very small non-threatening SSWC anomalies. The SSWC algorithm is currently being tested by one of the partners. In this test, all corrosion near the long seam is being investigated per US DOT regulatory requirements. Detailed measurements are being made at each excavation site to determine the presence of SSWC and the susceptibility of the pipe to this pipeline threat. The assessment is being performed with DOT PHMSA oversight.

**Mechanical Damage Sample Details.** A photograph of the dent with gouge, identified by classification algorithm, that was subjected to repeated pressurization to SMYS tested is shown in Figure 23. The maximum depth before pressure testing was 0.147 inch (0.74% of wall thickness) and after was nearly the same at 0.140 inch (0.70% of wall thickness). The dent depth in percent for the entire dent is shown in Figure 24.

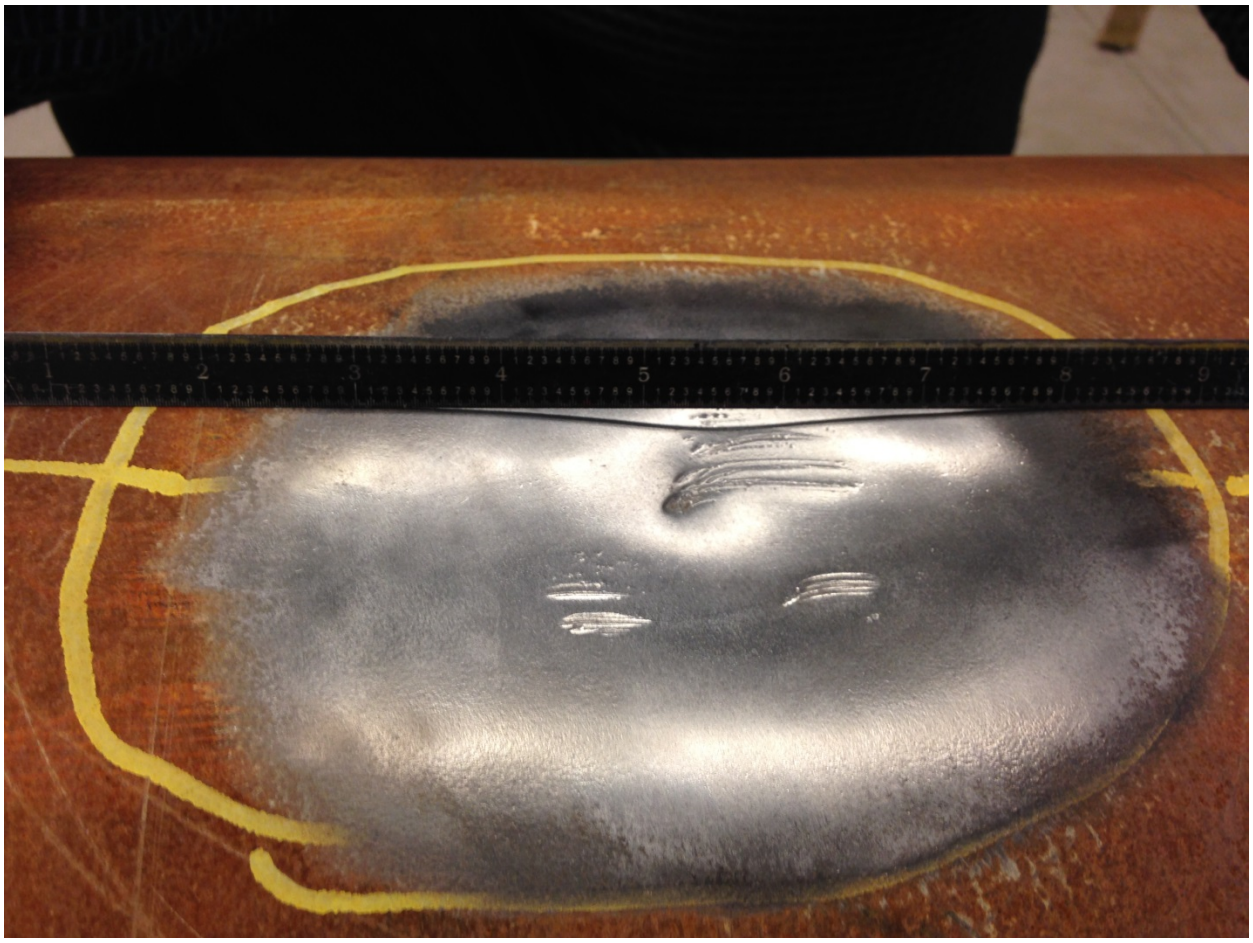

**Figure 23. Dent with gouge, identified by classification algorithm, that was subjected to repeated pressurization to SMYS**

| Circumferential Length (Inches) | 0.0 | 0.5 | 1.0 | 1.5 | 2.0 | 2.5 | 3.0 | 3.5 | 4.0 | 4.5 | 5.0 |
|---|---|---|---|---|---|---|---|---|---|---|---|
| | 0.01% | 0.01% | 0.03% | 0.07% | 0.06% | 0.06% | 0.08% | 0.06% | 0.06% | 0.06% | 0.06% |
| 4.5 | 0.00% | 0.01% | 0.03% | 0.04% | 0.06% | 0.07% | 0.08% | 0.08% | 0.08% | 0.07% | 0.05% |
| | 0.00% | 0.02% | 0.03% | 0.04% | 0.05% | 0.05% | 0.04% | 0.03% | 0.02% | 0.01% | 0.01% |
| 4.0 | 0.00% | 0.01% | 0.02% | 0.01% | 0.01% | 0.00% | 0.01% | 0.03% | 0.05% | 0.06% | 0.08% |
| | 0.00% | 0.01% | 0.01% | 0.01% | 0.01% | 0.00% | 0.02% | 0.04% | 0.07% | 0.10% | 0.12% |
| 3.5 | 0.00% | 0.00% | 0.00% | 0.01% | 0.02% | 0.03% | 0.07% | 0.11% | 0.12% | 0.20% | 0.22% |
| | 0.00% | 0.01% | 0.00% | 0.00% | 0.01% | 0.04% | 0.06% | 0.11% | 0.16% | 0.22% | 0.28% |
| 3.0 | 0.00% | 0.03% | 0.01% | 0.03% | 0.03% | 0.05% | 0.09% | 0.15% | 0.20% | 0.28% | 0.39% |
| | 0.00% | 0.00% | 0.01% | 0.02% | 0.03% | 0.06% | 0.09% | 0.16% | 0.23% | 0.31% | 0.43% |
| 2.5 | 0.00% | 0.00% | 0.01% | 0.02% | 0.01% | 0.06% | 0.11% | 0.19% | 0.26% | 0.36% | 0.49% |
| | 0.00% | 0.01% | 0.02% | 0.03% | 0.05% | 0.08% | 0.13% | 0.20% | 0.28% | 0.39% | 0.53% |
| 2.0 | 0.00% | 0.01% | 0.02% | 0.03% | 0.05% | 0.08% | 0.12% | 0.20% | 0.23% | 0.35% | 0.48% |
| | 0.00% | 0.01% | 0.01% | 0.03% | 0.04% | 0.07% | 0.11% | 0.18% | 0.24% | 0.32% | 0.41% |
| 1.5 | 0.00% | 0.00% | 0.01% | 0.02% | 0.03% | 0.06% | 0.10% | 0.17% | 0.23% | 0.26% | 0.35% |
| | 0.00% | 0.00% | 0.01% | 0.02% | 0.01% | 0.06% | 0.09% | 0.14% | 0.21% | 0.22% | 0.25% |
| 1.0 | 0.00% | 0.00% | 0.00% | 0.01% | 0.02% | 0.03% | 0.05% | 0.09% | 0.12% | 0.15% | 0.17% |
| | 0.00% | 0.00% | 0.01% | 0.01% | 0.01% | 0.00% | 0.02% | 0.04% | 0.06% | 0.08% | 0.10% |
| 0.5 | 0.02% | 0.00% | 0.01% | 0.01% | 0.02% | 0.02% | 0.01% | 0.00% | 0.02% | 0.04% | 0.06% |
| | 0.00% | 0.02% | 0.03% | 0.04% | 0.05% | 0.05% | 0.05% | 0.04% | 0.01% | 0.01% | 0.03% |
| 0.0 | 0.00% | 0.01% | 0.02% | 0.01% | 0.05% | 0.05% | 0.05% | 0.05% | 0.06% | 0.04% | 0.01% |

| Circumferential Length (Inches) | 0.0 | 0.5 | 1.0 | 1.5 | 2.0 | 2.5 | 3.0 | 3.5 | 4.0 | 4.5 | 5.0 |
|---|---|---|---|---|---|---|---|---|---|---|---|
| | 0.04% | 0.03% | 0.00% | 0.02% | 0.03% | 0.04% | 0.04% | 0.05% | 0.05% | 0.05% | |
| 4.5 | 0.03% | 0.02% | 0.01% | 0.01% | 0.01% | 0.01% | 0.01% | 0.00% | 0.00% | 0.01% | |
| | 0.01% | 0.03% | 0.03% | 0.03% | 0.03% | 0.01% | 0.00% | 0.01% | 0.01% | 0.01% | |
| 4.0 | 0.09% | 0.10% | 0.10% | 0.09% | 0.09% | 0.05% | 0.04% | 0.02% | 0.02% | 0.01% | |
| | 0.14% | 0.16% | 0.16% | 0.14% | 0.13% | 0.11% | 0.08% | 0.06% | 0.04% | 0.02% | |
| 3.5 | 0.23% | 0.22% | 0.20% | 0.17% | 0.14% | 0.11% | 0.07% | 0.05% | 0.02% | 0.03% | |
| | 0.32% | 0.33% | 0.32% | 0.28% | 0.24% | 0.19% | 0.13% | 0.09% | 0.05% | 0.02% | |
| 3.0 | 0.42% | 0.45% | 0.41% | 0.34% | 0.28% | 0.20% | 0.15% | 0.11% | 0.06% | 0.02% | |
| | 0.52% | 0.57% | 0.58% | 0.43% | 0.33% | 0.24% | 0.21% | 0.13% | 0.07% | 0.03% | |
| 2.5 | 0.62% | 0.66% | 0.58% | 0.48% | 0.38% | 0.26% | 0.26% | 0.13% | 0.07% | 0.02% | |
| | 0.70% | 0.70% | 0.62% | 0.53% | 0.41% | 0.28% | 0.19% | 0.13% | 0.07% | 0.03% | |
| 2.0 | 0.59% | 0.59% | 0.55% | 0.48% | 0.36% | 0.28% | 0.18% | 0.12% | 0.05% | 0.04% | |
| | 0.46% | 0.49% | 0.48% | 0.43% | 0.36% | 0.25% | 0.19% | 0.12% | 0.06% | 0.03% | |
| 1.5 | 0.38% | 0.40% | 0.44% | 0.41% | 0.33% | 0.24% | 0.17% | 0.11% | 0.05% | 0.02% | |
| | 0.29% | 0.31% | 0.31% | 0.31% | 0.27% | 0.21% | 0.16% | 0.10% | 0.06% | 0.04% | |
| 1.0 | 0.21% | 0.22% | 0.23% | 0.23% | 0.21% | 0.17% | 0.12% | 0.08% | 0.05% | 0.02% | |
| | 0.13% | 0.14% | 0.15% | 0.15% | 0.15% | 0.12% | 0.09% | 0.06% | 0.04% | 0.01% | |
| 0.5 | 0.08% | 0.10% | 0.11% | 0.12% | 0.11% | 0.09% | 0.07% | 0.05% | 0.03% | 0.00% | |
| | 0.05% | 0.06% | 0.07% | 0.06% | 0.06% | 0.09% | 0.02% | 0.01% | 0.05% | 0.00% | |
| 0.0 | 0.01% | 0.02% | 0.04% | 0.00% | 0.06% | 0.06% | 0.04% | 0.03% | 0.01% | 0.00% | |

**Axial Length (Inches)**

**Figure 24. The dent depth in percent**

**SSWC Burst Test Details.** In addressing the threat of SSWC, Kiefner examined six cut-out pipe pups with SSWC in our laboratory. These anomalies were identified by the inspection technology used for collecting the data for developing the SSWC classifier. Metallographs of three of the SSWC anomalies are shown in Figure 25 and Figure 26. Kiefner subjected the smallest detected SSWC flaw to a burst test. The pipe failed at a pressure of 3,340 psig and did not fail in the seam. This pressure exceeded that required to reach the pipe flow stress as calculated by (YS+UTS)/2 of 3,259 psig. Therefore Kiefner concluded that the ILI tool and classifier are capable of identifying very small non-threatening SSWC anomalies.

A second set of burst test were conducted to demonstrate that blunt corrosion crossing a seam weld in an operating pipeline is not more deleterious than blunt corrosion in the body of the pipe at least up to a seam Charpy transition temperature of 200°F. Two burst tests were

conducted: one with an EDM crack-like defect and another with an identical EDM defect but with a significant groove machined in it to simulate corrosion less deep than the tip of the crack-like defect, e.g., corrosion of the side walls of the notch near the external pipe surface. The groove anomaly is shown in Figure 27. It was expected that the defect with the groove would fail at an equal or higher pressure than the defect without the groove due to a reduction in the crack-tip stress intensity resulting from the stress contours being more spread out near the surface due to the grooving. This was confirmed by the EDM defect with the groove failing at a pressure 24 psig greater than the EDM defect without the groove as shown by the results in Table 4.

**Table 4. EDM Notch Burst Tests**

| | EDM Notch Dimensions | Buffing depth | Failure Pressure, psig |
|---|---|---|---|
| Without groove | 6” x 50% WT | 0 | 1,780 |
| With groove | 6” x 50% WT | 35% of WT | 1,804 |

Moreover, if corrosion of a LoF or hook crack were to occur and if it were to corrode sufficiently in depth to make the total defect deeper, it would be expected to corrode as a groove and look similar to SSWC and be detectable by ILI technology.

In summary, ILI methods can be used to conservatively identify locations of SSWC. The susceptibility of seam welds can be determined in the field. Blunt corrosion crossing a seam weld in an operating pipeline is not more deleterious than blunt corrosion in the body of the pipe at least up to a seam Charpy transition temperature of 200°F. This high of a transition temperature is associated with specific metallurgy which can be assessed in the field.

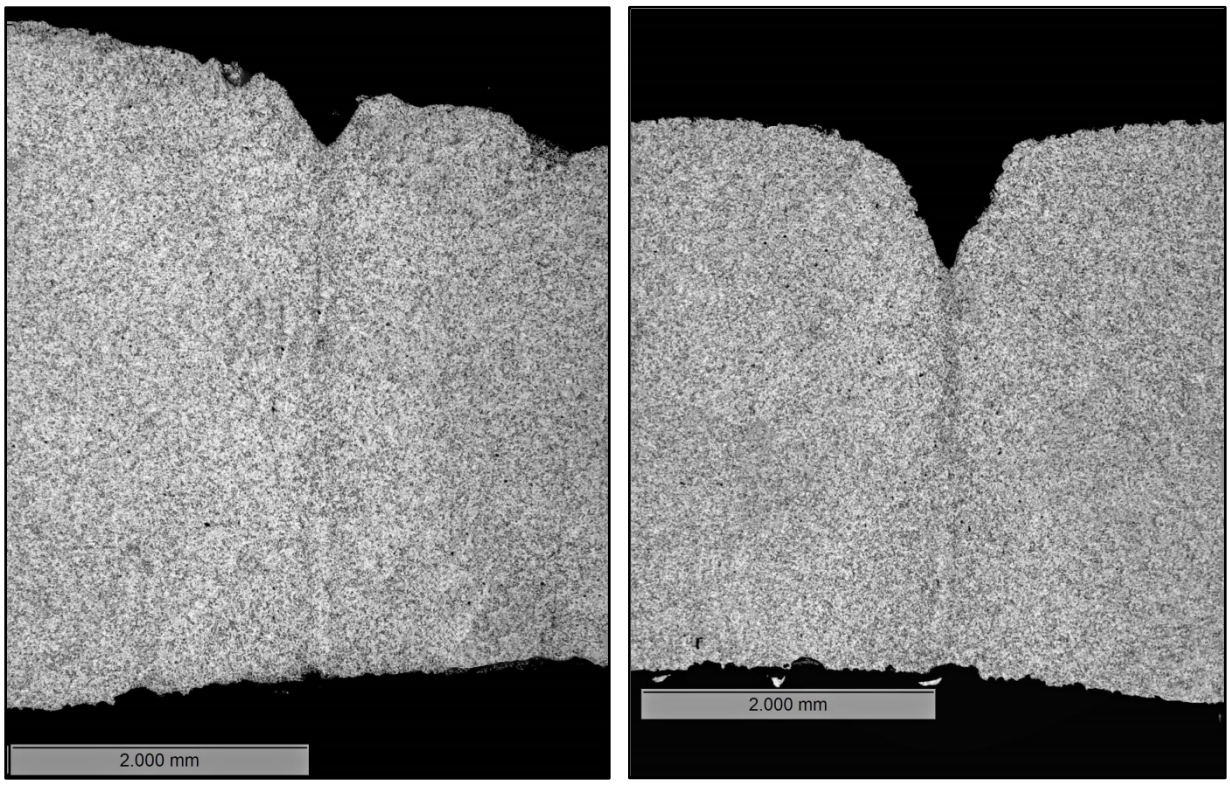


**Figure 25. Metallographic section through flaws G1 (left) and G5 (right)**

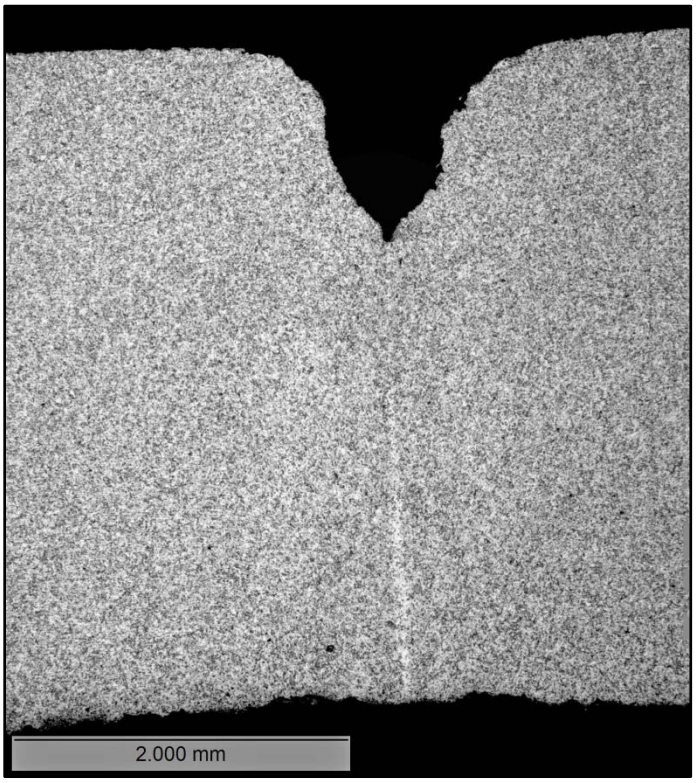


**Figure 26. Metallographic section through flaw G8 groove**

**Figure 27. Typical blunt machined groove**

# REFERENCES


1. Nestleroth, J.B. and Bubenik, T. A., Magnetic Flux Leakage (MFL) Technology for Natural Gas Pipeline Inspection, Battelle, Report Number GRI-00/0180 to the Gas Research Institute, February 1999.
2. Nestleroth, J.B. and Davis, R.J., "Stress, Cold Work, and Metal-Loss Induced Magnetic Flux Leakage Signals," Proceeding of the 11th PRCI-EPRG Joint Technical Meeting on Pipeline Research, PRC International, April 1997.
3. Dobmann, G. and Höller, P., "Physical Analysis Methods of Magnetic Flux Leakage," in Research Techniques in Nondestructive Testing, Volume IV, edited by R. S. Sharpe, Academic Press, 1980.
4. Atherton, David L., et al, "Stress Induced Magnetization Changes of Steel Pipes-Laboratory Tests," IEEE Transactions on Magnetics, Volume MAG-19, Number 4, July 1983.
5. Atherton, D. L., "Effect of Line Pressure on the Performance of Magnetic Inspection Tools," Oil & Gas Journal, October 27, 1986.
6. Nestleroth, J. B. and Crouch, A. E., *Variation of Magnetic Properties in Pipeline Steels*, Report No. DTRS56-96-C-0010, Subtask 1.1 Report, to the U. S. Department of Transportation, March 1998
7. Davis, R. J., et al., "The Feasibility Of Magnetic Flux Leakage In-Line Inspection as a Method To Detect and Characterize Mechanical Damage," GRI Report GRI-95/0369, 1996.
8. Davis, R. J. and Nestleroth, J. B., "The Feasibility of Using the MFL Technique to Detect and Characterize Mechanical Damage In Pipelines," *Review of Progress in Quantitative Nondestructive Evaluation*, Volume 16, Plenum New York, 1997.
9. Nestleroth, J.B., and Davis, R.J., "Pipeline Mechanical Damage Characterization By Multiple Magnetization Level Decoupling" *Review of Progress in Quantitative NDE*, Volume 18, Plenum New York, July 1998.
10. Bubenik, T.A., et al, "In-Line Inspection Technologies for Mechanical Damage and SCC in Pipelines – Final Report" Department of Transportation Report DTRS56-96-C-0010, June 2000.
11. Bubenik, T.A., J. B. Nestleroth, R. J. Davis, Lloyd Ulrich, and Harvey Haines, "Multiple Magnetization Level MFL For Pipeline Mechanical Damage Characterization" IPC00-0218 Proceedings of the International Pipeline Conference 2000, October 1-5, 2000, Calgary, Alberta, Canada.
12. Fact Sheet: Selective Seam Corrosion (SSC) Retrieved from //primis.phmsa.dot.gov/comm/FactSheets/FSSelectiveSeamCorrosion.htm, December 2011
13. Peter Massopust, Carl Torres, and Alan Dean, "Improving In-line Inspection for Mechanical Damage in Natural Gas Pipelines," PRCI, L52084, 2003.
14. Leo Breiman, "Random Forests," Machine Learning, vol. 45, no. 1, pp. 5-32, 2001.
15. Gareth James, An Introduction to Statistical Learning with Applications in R. New York, NY: Springer, 2013.
16. Murphy, K. (2012). *Machine Learning: A Probabilistic Perspective.* The MIT Press.
17. Pedregosa. (2011). Scikit-learn: Machine Learning in Python. *Journal of Machine Learning Research*, 2825-2830.

18. PHMSA “Comprehensive Study to Understand Longitudinal ERW Seam Failures”, PHMSA Contract No. DTPH56-11-T-000003, https://primis.phmsa.dot.gov/matrix/PrjHome.rdm?prj=390
19. PHMSA “Comprehensive Study to Understand Longitudinal ERW Seam Failures” Task3-2 Selective Seam Weld Corrosion Test Method , Brosia et al June 2013.

# ATTACHMENT A - FULL LISTING OF CLASSIFIER INPUTS AND PREDICTIONS USING OUT-OF-BAG SAMPLE

The following table is the full listing of classifier inputs and predictions using out-of-bag samples. Gold cells represent classifier errors that are conservative. Red cells represent classifier errors that are not conservative.

| Anomaly ID | Segment | ML Sig Location | ML Sig Count | ML Amp Ratio | ML Depth (%) | True Metal Loss Type | Predicted Metal Loss Type |
|---|---|---|---|---|---|---|---|
| 1 | Pipeline A | Shoulder | 4 | 0.91 | 9.1 | Corrosion | Corrosion |
| 2 | Pipeline A | Both | 13 | 1.71 | 12.5 | Corrosion | Corrosion |
| 3 | Pipeline A | Shoulder | 3 | 0.84 | 5.9 | Corrosion | Corrosion |
| 4 | Pipeline A | Shoulder | 3 | 1.13 | 6.3 | Corrosion | Corrosion |
| 5 | Pipeline A | Apex | 5 | 3.19 | 9.7 | None | Gouge |
| 6 | Pipeline A | Shoulder | 6 | 1.40 | 6.3 | Corrosion | Corrosion |
| 7 | Pipeline A | Apex | 2 | 2.24 | 1.0 | None | Gouge |
| 8 | Pipeline A | Apex | 2 | 1.47 | 7.9 | Gouge | Gouge |
| 9 | Pipeline A | Both | 6 | 1.31 | 4.3 | Corrosion | Corrosion |
| 10 | Pipeline A | Shoulder | 1 | 3.20 | 8.1 | Corrosion | Gouge |
| 11 | Pipeline A | Both | 10 | 2.94 | 11.0 | Corrosion | Corrosion |
| 12 | Pipeline A | Shoulder | 1 | 1.18 | 6.9 | None | Gouge |
| 14 | Pipeline A | Both | 2 | 0.81 | 1.7 | None | None |
| 15 | Pipeline A | Shoulder | 5 | 1.35 | 7.5 | Corrosion | Corrosion |
| 16 | Pipeline A | Both | 4 | 2.55 | 6.9 | Corrosion | Corrosion |
| 17 | Pipeline A | Both | 11 | 0.93 | 8.8 | Corrosion | Corrosion |
| 18 | Pipeline A | Apex | 1 | 0.55 | 3.0 | Gouge | Gouge |
| 19 | Pipeline A | Shoulder | 6 | 1.12 | 5.7 | Corrosion | Corrosion |
| 20 | Pipeline A | Shoulder | 3 | 0.94 | 7.9 | Corrosion | Corrosion |
| 21 | Pipeline A | Apex | 1 | 1.43 | 6.1 | None | Gouge |
| 23 | Pipeline A | Shoulder | 3 | 1.11 | 3.6 | Corrosion | Corrosion |
| 24 | Pipeline A | Both | 4 | 0.83 | 4.7 | Corrosion | Corrosion |
| 25 | Pipeline A | Both | 6 | 1.07 | 4.5 | Corrosion | Corrosion |
| 26 | Pipeline A | Both | 5 | 1.48 | 12.3 | Corrosion | Gouge |
| 27 | Pipeline A | Shoulder | 2 | 1.15 | 4.5 | Corrosion | Gouge |
| 28 | Pipeline A | Shoulder | 10 | 1.58 | 6.0 | Corrosion | Corrosion |
| 29 | Pipeline A | Apex | 1 | -0.42 | 5.1 | Gouge | Gouge |
| 30 | Pipeline A | Both | 5 | 2.06 | 4.2 | Corrosion | Corrosion |
| 31 | Pipeline A | Both | 5 | 1.21 | 2.7 | None | Corrosion |
| 32 | Pipeline A | Shoulder | 1 | 1.56 | 5.3 | Corrosion | Gouge |
| 33 | Pipeline A | Both | 10 | 1.36 | 7.9 | Corrosion | Corrosion |
| 34 | Pipeline A | Shoulder | 2 | 1.26 | 5.4 | Corrosion | Gouge |
| 35 | Pipeline A | Both | 6 | 2.55 | 17.8 | None | Corrosion |
| 36 | Pipeline A | Apex | 1 | 0.90 | 3.3 | Gouge | Gouge |
| 37 | Pipeline A | Apex | 1 | 1.52 | 4.8 | Gouge | Gouge |
| 38 | Pipeline A | Apex | 1 | 0.88 | 7.8 | Gouge | Gouge |
| 40 | Pipeline A | Apex | 4 | 4.85 | 4.8 | Corrosion | Gouge |

| Anomaly ID | Segment | ML Sig Location | ML Sig Count | ML Amp Ratio | ML Depth (%) | True Metal Loss Type | Predicted Metal Loss Type |
|---|---|---|---|---|---|---|---|
| 42 | Pipeline A | Both | 2 | 0.59 | 7.9 | None | Gouge |
| 43 | Pipeline A | Apex | 1 | 0.88 | 9.7 | Gouge | Gouge |
| 44 | Pipeline A | Apex | 1 | 0.77 | 8.7 | Gouge | Gouge |
| 45 | Pipeline E | Apex | 1 | 1.98 | 20.0 | Gouge | Gouge |
| 46 | Pipeline E | Apex | 1 | 2.26 | 16.4 | Gouge | Gouge |
| 47 | Pipeline E | Apex | 1 | 1.31 | 10.0 | None | Gouge |
| 48 | Pipeline E | Apex | 1 | 0.80 | 10.0 | None | Gouge |
| 49 | Pipeline E | Both | 2 | 1.49 | 10.0 | Gouge | Gouge |
| 50 | Pipeline E | Both | 4 | 1.43 | 10.0 | Gouge | Corrosion |
| 51 | Pull Test | Apex | 1 | 1.65 | 3.9 | Gouge | Gouge |
| 52 | Pull Test | Apex | 1 | 1.62 | 7.6 | Gouge | Gouge |
| 53 | Pull Test | Apex | 2 | 2.15 | 11.5 | Gouge | Gouge |
| 54 | Pull Test | Shoulder | 1 | 0.51 | 4.2 | Gouge | Gouge |
| 55 | Pull Test | Apex | 1 | 1.93 | 8.4 | Gouge | Gouge |
| 56 | Pull Test | Apex | 1 | 1.21 | 8.4 | Gouge | Gouge |
| 57 | Pull Test | Shoulder | 1 | 0.32 | 8.5 | Gouge | Gouge |
| 58 | Pull Test | Apex | 1 | 2.42 | 5.1 | Gouge | Gouge |
| 59 | Pull Test | Apex | 1 | 0.70 | 8.6 | Gouge | Gouge |
| 60 | Pull Test | None | 0 | 0.00 | 0.0 | None | None |
| 61 | Pull Test | Both | 2 | 4.20 | 4.4 | Gouge | Gouge |
| 62 | Pull Test | None | 0 | 0.00 | 0.0 | None | Gouge |
| 63 | Pull Test | Apex | 1 | 3.56 | 15.3 | Gouge | Gouge |
| 64 | Pull Test | None | 0 | 0.00 | 0.0 | None | None |
| 65 | Pull Test | Apex | 1 | 2.32 | 12.9 | Gouge | Gouge |
| 66 | Pull Test | Apex | 1 | 1.70 | 10.6 | Gouge | Gouge |
| 67 | Pull Test | Apex | 1 | 2.65 | 4.7 | Gouge | Gouge |
| 68 | Pull Test | Apex | 1 | 2.45 | 7.8 | Gouge | Gouge |
| 69 | Pull Test | Apex | 3 | 3.55 | 8.8 | Gouge | Gouge |
| 70 | Pull Test | Apex | 1 | 1.91 | 21.8 | Gouge | Gouge |
| 71 | Pull Test | Apex | 3 | 2.58 | 11.9 | Gouge | Gouge |
| 72 | Pull Test | Apex | 1 | 4.46 | 8.9 | Gouge | Gouge |
| 73 | Pull Test | Apex | 2 | 1.79 | 6.7 | Gouge | Gouge |
| 74 | Pull Test | None | 0 | 0.00 | 0.0 | None | None |
| 75 | Pull Test | Apex | 1 | 0.98 | 7.9 | Gouge | Gouge |
| 76 | Pull Test | Apex | 1 | 1.30 | 5.9 | Gouge | Gouge |
| 77 | Pull Test | Apex | 2 | 1.22 | 16.4 | Gouge | Gouge |
| 78 | Pull Test | Apex | 1 | 1.63 | 7.7 | Gouge | Gouge |
| 79 | Pull Test | Apex | 2 | 1.64 | 8.4 | Gouge | Gouge |
| 80 | Pull Test | Apex | 1 | 2.07 | 15.8 | Gouge | Gouge |
| 81 | Pull Test | Shoulder | 1 | 1.28 | 4.7 | Gouge | Gouge |

| Anomaly ID | Segment | ML Sig Location | ML Sig Count | ML Amp Ratio | ML Depth (%) | True Metal Loss Type | Predicted Metal Loss Type |
|---|---|---|---|---|---|---|---|
| 82 | Pull Test | Apex | 1 | 0.81 | 3.9 | Gouge | Gouge |
| 83 | Pull Test | Apex | 1 | 2.80 | 3.9 | Gouge | Gouge |
| 84 | Pull Test | Apex | 2 | 2.62 | 10.0 | Gouge | Gouge |
| 85 | Pull Test | Apex | 3 | 1.64 | 7.0 | Gouge | Gouge |
| 86 | Pull Test | Apex | 2 | 1.92 | 9.7 | Gouge | Gouge |
| 87 | Pull Test | Apex | 2 | 1.32 | 21.1 | Gouge | Gouge |
| 88 | Pull Test | Apex | 2 | 0.94 | 9.0 | Gouge | Gouge |
| 89 | Pull Test | Apex | 1 | 1.64 | 10.0 | Gouge | Gouge |
| 90 | Pull Test | None | 0 | 0.00 | 0.0 | Gouge | None |
| 91 | Pull Test | Apex | 1 | 0.67 | 10.0 | Gouge | Gouge |
| 92 | Pull Test | Apex | 1 | 2.11 | 7.2 | Gouge | Gouge |

# ATTACHMENT B - DETAILED DATA AND RESULTS FOR SSWC MODEL DEVELOPMENT

## Table B1. Anomalies for model development

| Segment | Dig | ILI Group ID | ILI Log Distance (ft) | ILI Corrosion Depth (%) | SSWC? | SSWC Length (Inches) | SSWC Depth (%) |
|---|---|---|---|---|---|---|---|
| "B" | 13-1605 | 40000500 | 332.78 | | 1 | 0.70 | 27.7% |
| "B" | 13-1605 | 40000503 | 333.01 | | 1 | 1.70 | 26.6% |
| "B" | 13-1606 | 40013090 | 4028.92 | | 1 | 2.80 | 38.3% |
| "B" | 13-1606 | 40013056 | 4018.32 | 13.0% | 0 | | |
| "B" | 13-1606 | 40013057 | 4018.78 | 13.0% | 0 | | |
| "B" | 13-1611 | 40031011&12 | 11513.17 | | 1 | 2.50 | 14.9% |
| "B" | 13-1611 | 40031015 | 11513.69 | | 1 | 1.00 | 22.2% |
| "B" | 13-1611 | 40031031 | 11516.74 | 14.0% | 0 | | |
| "B" | 13-1611 | 40031035 | 11516.95 | 18.0% | 0 | | |
| "B" | 13-1617 | 40065422 | 30201.89 | | 1 | 0.40 | 38.1% |
| "B" | 13-1617 | 40065424 | 30202.45 | 23.0% | 0 | | |
| "B" | 13-1617 | 40065492 | 30225.05 | | 1 | 0.60 | 44.2% |
| "B" | 13-1617 | 40065506 | 30225.92 | 30.0% | 0 | | |
| "B" | 13-1617 | 40065507 | 30225.99 | 12.0% | 0 | | |
| "B" | 13-1617 | 40065532-35 | 30228.09 | 20.0% | 0 | | |
| "B" | 13-1630 | 40301147 | 122718.35 | | 1 | 1.00 | 31.7% |
| "B" | 13-1630 | 40301164 | 122728.44 | | 1 | 2.00 | 39.5% |
| "B" | 13-1630 | 40301165 | 122728.71 | 18.0% | 0 | | |
| "B" | 13-1630 | 40301169 | 122729.55 | 12.0% | 0 | | |
| "B" | 13-1630 | 40301174-5 | 122733.94 | 10.0% | 1 | 1.50 | 20.7% |
| "B" | 13-1630 | 40301180 | 122736.51 | 14.0% | 0 | | |
| "B" | 13-1630 | 40301191 | 122741.87 | 33.0% | 0 | | |
| "B" | 13-1630 | 40301198 | 122746.23 | | 1 | 1.50 | 35.8% |
| "B" | 13-1631 | 40304840 | 124978.63 | | 1 | 3.00 | 41.7% |
| "B" | 13-1631 | 40304842 | 124979.16 | | 1 | 0.50 | 23.5% |
| "C" | 13-1280 | | 3026.95 | 15.0% | 0 | | |
| "C" | 13-1281 | 40004225 | 4731.55 | 16.0% | 0 | | |
| "C" | 13-1282A | 40005395 | 9254.93 | 22.0% | 0 | | |
| "C" | 13-1282B | 40005396 | 9255.94 | 12.0% | 0 | | |
| "C" | 13-1282C | 40005397 | 9257.58 | 17.0% | 0 | | |
| "C" | 13-1283A | 40006669 | 10278.93 | 14.0% | 0 | | |
| "C" | 13-1283B | 40006678 | 10277.86 | 16.0% | 0 | | |
| "C" | 13-1283C | 40006686 | 10278.87 | 18.0% | 0 | | |
| "C" | 13-1283D | 40006752 | 10295.78 | 21.0% | 0 | | |
| "C" | 13-1284 | 40006808 | 10328.59 | 24.0% | 0 | | |
| "C" | 13-1285A | 40007095 | 10545.51 | 19.0% | 0 | | |
| "C" | 13-1285B | 40007147 | 10574.17 | 30.0% | 0 | | |
| "C" | 13-1286 | 40007241 | 10638.59 | 14.0% | 0 | | |
| "C" | 13-1287 | 40015549 | 63545.12 | 34.0% | 0 | | |

**Table B2. Classifier accuracy results: Three false negatives and two false positives.**

| ILI Corrosion Depth (%) | Truth: SSWC? | Classifier Probability of SSWC | SSWC Length (Inches) | SSWC Depth (%) |
|---|---|---|---|---|
| | 1 | 0.532 | 0.70 | 27.7% |
| | 1 | 0.996 | 1.70 | 26.6% |
| | 1 | 0.918 | 2.80 | 38.3% |
| 13.0% | 0 | 0.029 | | |
| 13.0% | 0 | 0.321 | | |
| | 1 | 0.424 | 2.50 | 14.9% |
| | 1 | 0.229 | 1.00 | 22.2% |
| 14.0% | 0 | 0.011 | | |
| 18.0% | 0 | 0.096 | | |
| | 1 | 0.975 | 0.40 | 38.1% |
| 23.0% | 0 | 0.164 | | |
| | 1 | 0.969 | 0.60 | 44.2% |
| 30.0% | 0 | 0.089 | | |
| 12.0% | 0 | 0.010 | | |
| 20.0% | 0 | 0.008 | | |
| | 1 | 0.871 | 1.00 | 31.7% |
| | 1 | 0.962 | 2.00 | 39.5% |
| 18.0% | 0 | 0.164 | | |
| 12.0% | 0 | 0.761 | | |
| 10.0% | 1 | 0.212 | 1.50 | 20.7% |
| 14.0% | 0 | 0.059 | | |
| 33.0% | 0 | 0.893 | | |
| | 1 | 0.923 | 1.50 | 35.8% |
| | 1 | 0.927 | 3.00 | 41.7% |
| | 1 | 0.676 | 0.50 | 23.5% |
| 15.0% | 0 | 0.143 | | |
| 16.0% | 0 | 0.069 | | |
| 22.0% | 0 | 0.020 | | |
| 12.0% | 0 | 0.054 | | |
| 17.0% | 0 | 0.015 | | |
| 14.0% | 0 | 0.089 | | |
| 16.0% | 0 | 0.046 | | |
| 18.0% | 0 | 0.008 | | |
| 21.0% | 0 | 0.027 | | |
| 24.0% | 0 | 0.014 | | |
| 19.0% | 0 | 0.084 | | |
| 30.0% | 0 | 0.009 | | |
| 14.0% | 0 | 0.024 | | |
| 34.0% | 0 | 0.178 | | |